NUCLEAR MATERIALS / JANUARY 2018

PASSIVE NEUTRON ALBEDO REACTIVITY IN THE FINNISH ENCAPSULATION CONTEXT

Stephen J. Tobin, Pauli Peura, Tapani Honkamaa, Peter Dendooven, Mikael Moring, Camille Bélanger-Champagne

Säteilyturvakeskus
Strålsäkerhetscentralen
Radiation and Nuclear Safety Authority

STUK

Finnish Nuclear and Safety Authority
PL 14
00881 Helsinki
www.stuk.fi

Additional information
Tapani Honkamaa
tapani.honkamaa@stuk.fi

ISBN 978-952-309-406-2 (pdf)

Table of Contents

1 Introduction

The purpose of this report is to document the Monte Carlo simulation and analytic results for the implementation of the Passive Neutron Albedo Reactivity (PNAR) nondestructive assay (NDA) technique in the context of Finnish spent fuel encapsulation needs. This document is offered as partial fulfillment of the contract between Encapsulation NDA Services and Radiation and Nuclear Safety Authority (STUK) of Finland. The end goal of this research effort is two conceptual designs of the PNAR technique for both BWR and PWR fuel in Finland.

2 Description of the Research Process

The creation of a conceptual PNAR design involves making decisions on many interrelated design variables. For this reason, an initial design will be simulated and analyzed to fruition. Then changes or perturbations to the simulated design will be recommended for the final design. Some of the factors that must be considered are listed here:

1. The neutron detector material (3He or boron) must be protected from the inherent gamma flux to assure that the measured signal is only measuring neutrons. Fission chambers will also be researched but they do not need gamma protection.
2. The neutron count rate cannot exceed the count rate limits of the currently available technology, nor can the count rate be so low that the counting time is unacceptably long or the statistics unacceptably poor.
3. The uncertainty caused by factors such as fuel positioning in the detector should be minimized to reduce their impact on the instrument's sensitivity. The instrument design impacts the uncertainty and, at the same time, is dependent on the uncertainty. For example, it is desirable to design the instrument such that the count rate does not limit the sensitivity of the instrument; yet, there is no benefit to an elevated count rate if other uncertainties limit the sensitivity.
4. For the VVER fuel, the boron content of the water will vary which will impact the uncertainty of the PNAR measurement.

Given that there are several interrelated parameters, which need to be selected, as well as uncertainties outside the control of the NDA system, the current research effort started with a design based on experience. This initial design is being advanced to fruition. Yet, it is important to not lose sight of the interrelation of design features. We anticipate upfront that the final design recommendations will deviate somewhat from the simulations performed in this report.

3 Passive Neutron Albedo Reactivity

The Passive Neutron Albedo Reactivity (PNAR) Technique was first researched in 1982 although the acronym PNAR was not used at that time. [1] [2] [3] [4] [5] The general concept of interest to this study involves measuring the neutron flux from an assembly twice and comparing the two measurements by taking the ratio of these measurements. The change in the ratio measured for a given assembly type is proportional to the change in the reactivity of the assembly. In one measurement, the fuel is surrounded by material that maximizes the neutron multiplication, while in the second measurement the setup minimizes the neutron multiplication. This comparison of two measurements provides the assurance that fissile material is present in a spent fuel assembly.

In the context of much of the accessible spent fuel, which is generally stored in water, the high multiplying case is the assembly in water. Recalling that cadmium (Cd) is a material with a relatively low absorption cross section for neutrons above ~0.5 eV and a very high absorption cross section for neutrons below ~0.5 eV, the low multiplying case can be created by placing a one millimeter thick Cd-liner as close as possible to the assembly; ~5 mm separation between the fuel and the Cd is generally possible. This Cd needs to extend in the axial direction for 0.4 to 0.7 meters to significantly modify the multiplication over a section of fuel. The detectors are located near the axial midpoint of the Cd. [4]

Traditionally, the PNAR Ratio is calculated by dividing the count rate measured with the detectors in the high multiplying section by the count rate measured in the low multiplying section. The detector units were designed to detect epithermal neutrons, neutrons with an energy above 0.5 eV. Yet, the actual detection material (^{3}He, ^{235}U or boron) is primarily detecting thermal neutrons. The energy filtering is achieved by placing the detection tubes in polyethylene (PE) blocks surrounded by a Cd layer. Once the neutrons have penetrated through the Cd layer, the neutrons that thermalize in the PE block have the largest detection probability.

For the **primary PNAR design** approach presented in this study, the only physical difference in the setup between high and low multiplying sections is the presence or absence of one millimeter of Cd around the fuel. To think about the impact of the Cd-liner, it is helpful to divide the neutron energy spectrum into two parts:

1. The neutrons at the Cd-liner, which are above ~0.5 eV, are unaffected by the presence of the Cd. As such any counts created by these high-energy neutrons are included in both the numerator and denominator of the PNAR Ratio.
2. The neutrons at the Cd-liner, which are below ~0.5 eV, are affected by the presence of the Cd. When the Cd is absent these neutrons travel to and from the fuel boundary region inducing a certain amount of fission that spreads throughout the assembly. When the Cd is present, all such induced fission, caused by the low energy neutrons crossing the layer where the Cd is, do not take place.

This second point listed above is the reason why the PNAR technique is sometimes described as **interrogating the fuel with low energy neutrons from the location of the Cd-liner**. The measured count rate in the numerator of the PNAR Ratio includes the counts created by the fission chains that resulted from low-energy neutrons returning from the water to the fuel. In the case of the denominator's count rate, the low energy neutrons absorbed by the Cd-liner do not contribute.

The decision to wrap the PE, in which the neutron detectors are located, with Cd is a separate decision from the use of Cd to change the multiplication of the assembly. By surrounding the neutron detector with Cd, the high-energy neutrons or epithermal neutrons from the fuel are being selected preferentially for detection. The PNAR Ratio will work with or without the inclusion of Cd around the neutron detectors. It was decided to include Cd around the neutron detector because the high-energy neutrons arriving at the detector come from deeper in the assembly, a positive attribute that was demonstrated in the preliminary PNAR research performed by Lee and Lindqvist, which demonstrated that the epithermal neutron detectors were more uniformly sensitive to neutrons throughout the assembly. [1] By placing Cd around the detector, the low energy interrogating flux is not directly detected, rather only neutrons produced in the multiplying chain

caused by the low energy neutrons, which are born with an energy represented by the Watt Fission Spectrum, can be detected.

4 PNAR's Role in a Safeguards System

The PNAR instrument is expected to be used as part of an integrated NDA system. Per discussions with the responsible authorities, we currently anticipate that a PNAR instrument will be integrated with a Passive Gamma Emission Tomography (PGET) instrument. [6] Additionally, a computational component is expected to also be used that includes two simulation codes: (a) the Standardized Computer Analyses for Licensing Evaluation (SCALE) code [7] for simulating the irradiation in the fuel and (b) the Monte Carlo N-Particle Code, Version 6, (MCNP6™) [8] for transport neutrons and gammas to the NDA detectors. The term "and/or" is used below in the context of the gamma information because it is currently not clear if the SCALE simulations will use the current measured by the ion chambers, which are expected to be included in the PNAR instrument, or if the SCALE simulations will use the ^{137}Cs signal generated by PGET, or other information, measured by the PGET. Because the fuel is over 20-years cooled the difference between the ion chamber current and the ^{137}Cs signal is small.

The following is a discussion of the role of a PNAR instrument in the anticipated integrated NDA system (PGET + PNAR + total neutron {part of PNAR} + gross gamma [{from ion chambers in PNAR} and/or {total ^{137}Cs intensity from PGET}]). This NDA system will satisfy the requirements recommended by the NDA Experts Group working within the context of the IAEA's sponsored ASTOR group. [9] For a system combining PGET and PNAR, all the necessary hardware is available to enable the comparison that Euratom has developed with Oak Ridge National Laboratory researchers that includes SCALE and MCNP6™ calculations, [10] which would be used to compare the declaration and the measured signals (neutron, gamma {^{137}Cs and/or gross gamma} and multiplication):

1. The primary role of PNAR is to assure the inspectorate that a given assembly is multiplying at a rate consistent with the assemblies' declaration - to show that the expected amount of fissile material is present.
2. For the cases when PGET cannot see every pin, PNAR, along with the gamma and total neutron measurements combine to provide diversion detection capability. The detection of individual pins is not expected to be possible with this approach but a lower, more robust detection limit is expected relative to total neutron and gamma measurements alone.
3. In summary - the PNAR instrument strengthens the capability of the integrated NDA system because each declared assembly would need to satisfy each of the following:
    a) Emit ^{137}Cs or ^{154}Eu rays from every pin for BWR assemblies, or nearly every pin for VVER assemblies, within some range of absolute intensity (photon/s) and within an expected range of relative intensity.
    b) Emit neutrons at an intensity (neutrons/s) consistent with the declaration.
    c) Emit gross gamma with an intensity (current in ion chamber) consistent with the declaration.
    d) Multiplying at a level consistent with the declaration.

5 BWR and VVER PNAR Design

In Figure 1 and Figure 2, the vertically and horizontally cross-cutting images of the PNAR design used in the simulation of neutrons and gammas from Boiling Water Reactor (BWR) assemblies [11] are illustrated. In Figure 3 and Figure 4 similar vertically and horizontally cross-cutting images depict the design used with Water-Water Energetic Reactor (VVER) assemblies. [12] In Figure 5 image of two detectors located on opposite sides of a VVER assembly is shown to indicate the relative position of detectors, which are not situated on the same elevation. Both the BWR and the VVER design have detectors located at two closely located vertical levels; this design choice was made to have the same detection efficiency on all sides of the assembly and to enable future research into the possibility of reducing the number of detectors. It is likely that a PNAR design can be implemented with detectors located on one level without degrading the performance significantly; a change which would reduce the Cd-liner length by 10 cm.

The location of Cd in the various images is particularly important: (1) Cd in the shape of a long, thin vertical liner creates the low multiplying section of the detector and (2) Cd surrounds the PE structure in which the neutron detector, ^{3}He in the case of Figure 1 to Figure 5 is located. The Cd-liner located alongside the fuel is present in all the images. Yet, when simulating the high multiplying case, this 1 mm layer of Cd is replaced with 1 mm of steel. Of note, in the VVER design illustrated in Figure 5, the neutron detector resides inside of a large block of PE. The motivation for including the PE was to increase the multiplication of the high multiplying section as well as to minimize the impact of variation of the boron content in the water. Simulations were also performed for which the PE was replaced with borated water. In Table 1, some of the key parameters of the PNAR design are listed.

The use of flat surfaces in the BWR detector design was selected to simplify fabrication, while the use of cylindrical surfaces with the VVER design was selected to reduce the mass of the design, as well as to slightly improve the PNAR physics by reducing the perturbation that the detectors cause in the high multiplying section. The detector perturbs the high multiplying section by introducing Cd close to the fuel.

The PNAR instrument must work for all assemblies that are likely to be measured; yet, the shielding calculations described in the next section only need to be simulated for the worst-case assembly as the shielding for all other assemblies will be more than sufficient. For all the BWR simulation results, the response from four detectors were combined, while for the VVER simulations the results for 6 tubes were combined. In Figure 2 only two detectors are visible. In Figure 5 the positioning of detectors at two vertical levels is depicted for the VVER design. To accommodate the presence of detectors at two different elevations, the Cd-liner was increased in length to a total length of 0.74 m. The length of the Cd-liner was selected such that it extends vertically ~0.3 m above the active length of the nearest ^{3}He tube [4]. A few simulations were performed for which the Cd-liner was extended 0.23 m further up and down to quantify how much this might improve the sensitivity of the PNAR results. The meaning of the term sensitivity in this context is the amount that the PNAR Ratio changes for a given change in the multiplication of the assembly.

When simulating BWR assemblies, the count rate from each 40-mm sub-section of the ^{3}He tube was tallied separately so that the utility of using 40, 120 and 200 mm length tubes could be assessed. In Figure 2 the 40 mm long cylinders of ^{3}He are visible. Similarly, when VVER assemblies

were simulated, the count rate from each 20-mm sub-section of the ^{3}He tube was tallied separately so that the utility of using 20, 60 and 100 mm length tubes could be assessed as is illustrated in Figure 4

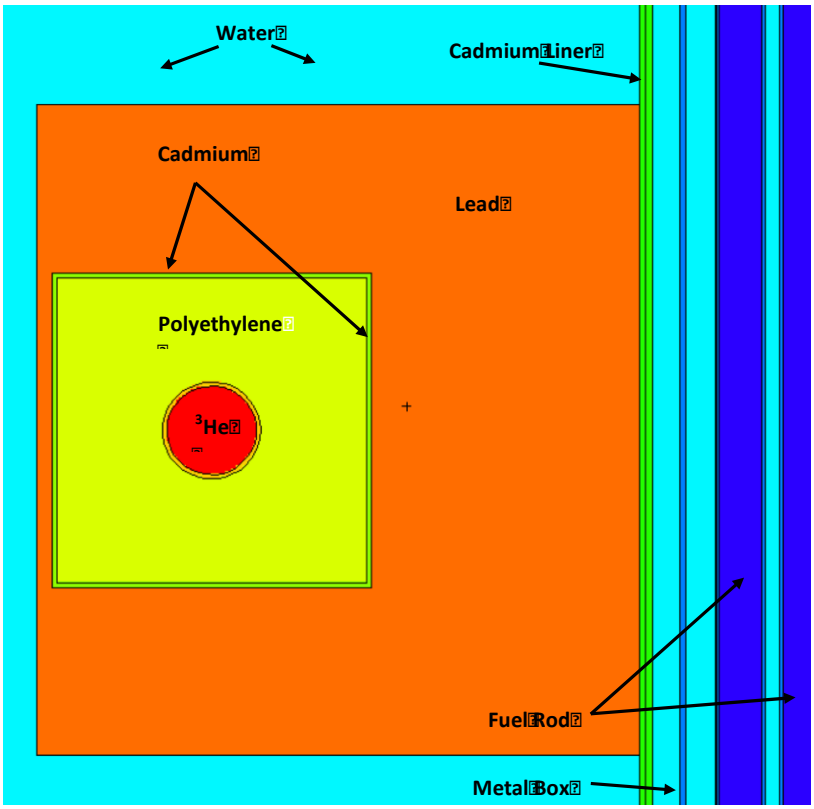

Figure 1, vertical (XZ plane) cross-sectional view of the BWR PNAR detector along one side of a BWR fuel assembly. Relative proportions are accurate.

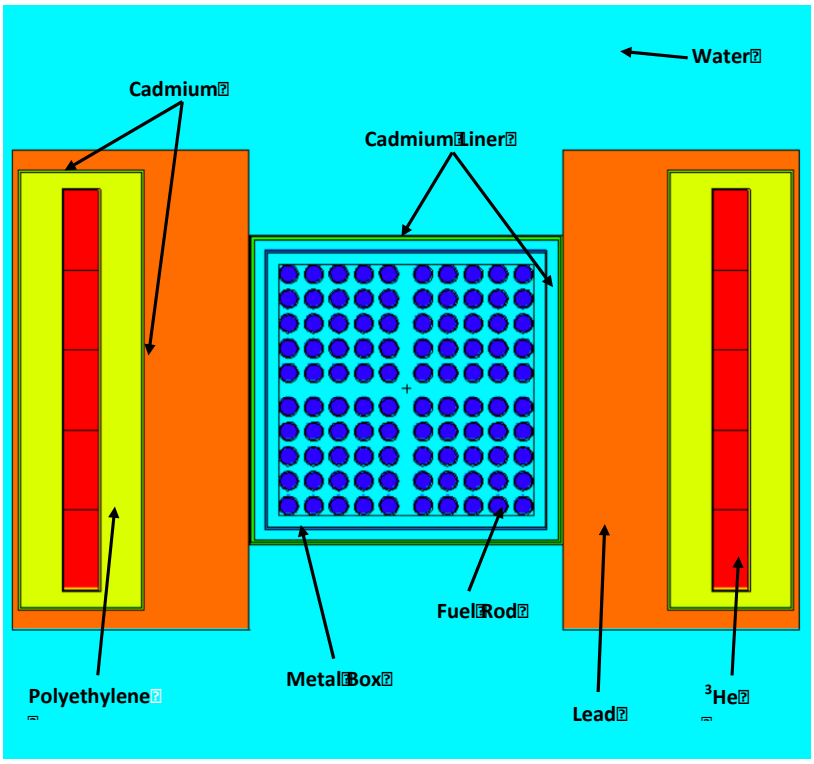

Figure 2, horizontal (XY plane) cross-sectional view of the BWR PNAR detector relative to a 10x10 BWR fuel assembly. Relative proportions are accurate.

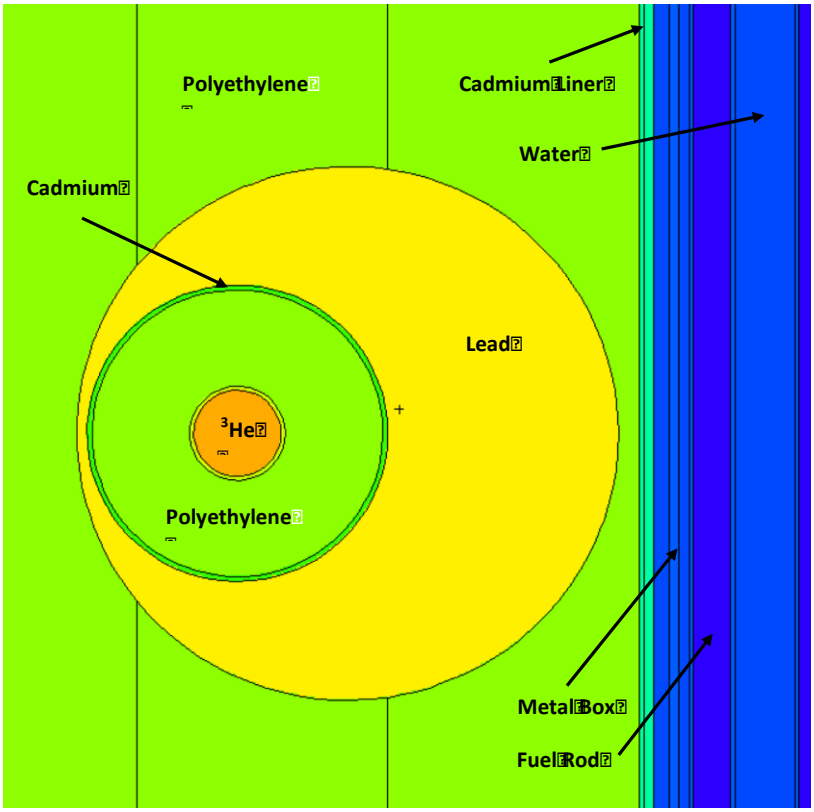

Figure 3, vertical (XZ plane) cross-sectional view of the VVER PNAR detector along one side of a VVER fuel assembly. Relative proportions are accurate.

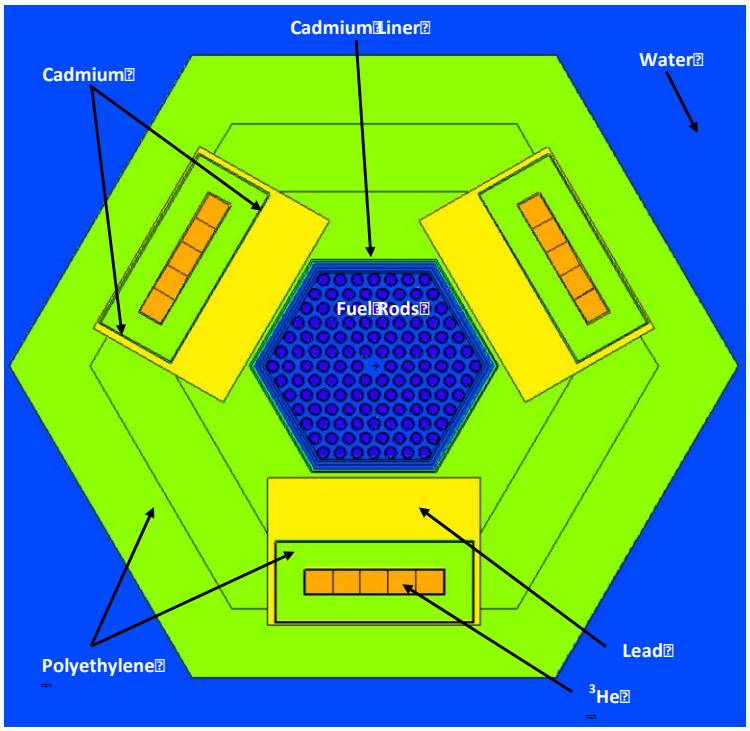

Figure 4, horizontal (XY plane) cross-sectional view of the VVER PNAR detector along one side of a VVER fuel assembly. Relative proportions are accurate.

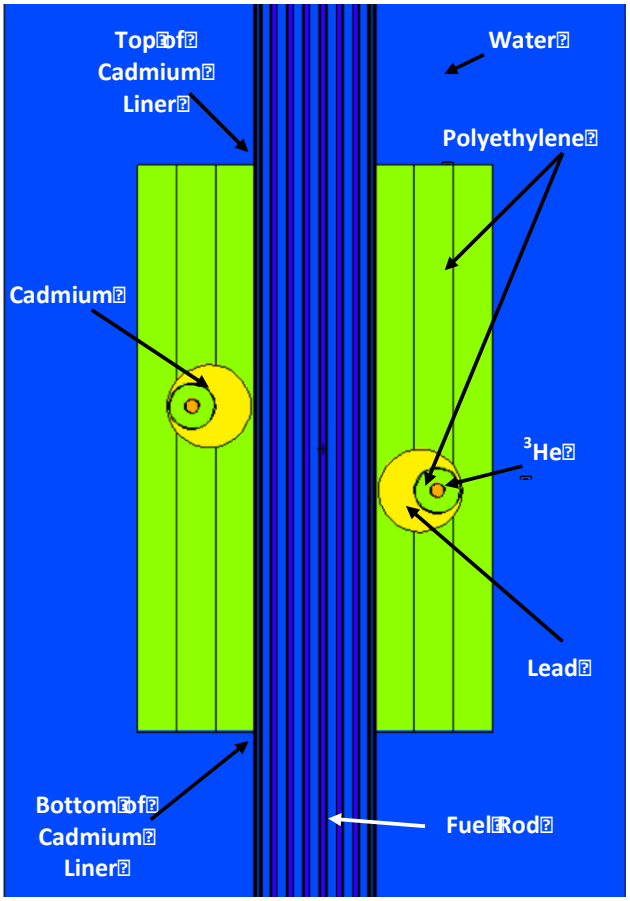

Figure 5, enlarged vertical (XZ plane) cross-section of Figure 3 indicating two VVER PNAR detector along two sides of a VVER fuel assembly. Relative proportions are accurate.

Design Features	BWR	VVER
^{3}He DIAMETER (MM)	17.4	17.4
^{3}He PRESSURE (ATM)	6.0	6.0
^{3}He LENGTHS OF TALLIED SECTION OF ^{3}He (MM)	40, 120, 200	20, 60, 100
PE BLOCK, OR DIAMETER AND LENGTH (MM)	60X60X218	D= 58, L=142
LEAD BLOCK, OR DIAMETER AND LENGTH (MM)	117X128X240	D=108, L=154
THICKNESS OF Cd AROUND PE AND IN THE LINER AROUND THE ASSEMBLY (MM)	1.0	1.0
VERTICAL EXTENT OF Cd-LINER SURROUNDING FUEL (M)	0.74	0.74
MINIMAL THICKNESS Pb, FUEL TO PE (MM)	52	46
THICKNESS Pb ABOVE AND BELOW PE BLOCK (MM)	33	NA

Table 1, list of detector parameters used to create the designs illustrated in Figure 1 through Figure 5.

6 Gamma Simulation for PNAR Design

Several gamma simulations were performed in the process of arriving at the design illustrated in Figure 1 to Figure 5 during which the gamma dose (Gy/hr or Rad/hr) to the tubes was tallied. The technical details for the gamma simulations are given in Appendix A. The dimensions of the lead block and the position of the PE section within the lead were selected based upon the gamma simulations. With the BWR design, the side of the lead through which each gamma entered the lead was tallied to balance the direction from which the dose was received by the ^{3}He gas among the various sides of the detector.

The starting point for the PNAR design involved gamma simulations because the dose to the ^{3}He tubes must be sufficiently low to assure that only neutrons contribute significantly to the measured count rate. The following variables impact the gamma tolerance of a ^{3}He tube: active length, fill pressure, tube diameter, irradiated gamma-ray spectrum and quenching gas. Research varying these parameters is given in publications. [13] [14] A case that was measured, which is close to the case likely to be used in Finland, is the following: 0.356 m active length, 4 atm fill pressure, 25 mm diameter tube, N_2 fill gas. This case was irradiated with a ^{226}Ra source and the neutron count rate was not altered until the gamma dose surpassed 0.2 Gy/hr (20 Rad/hr). The case simulated for the current work was selected through discussions with Nathan Johnson of GE Reuter-Stokes who is a co-author on both references. [13] [14] The ^{3}He tube selected for this study had an active length of 0.20 m, fill pressure of 6 atm, a tube diameter of 17.4 mm and N_2 as a quench gas. For the design used in the current study, the tube has a shorter length, reduced tube diameter and

will experience a softer gamma spectrum than in the published work, rendering it more tolerant to gamma irradiation. The increase in the ^{3}He pressure from 4 to 6 atmospheres makes the selected case less tolerant. In aggregate, based on the data listed in both the references, the tube being used in this publication should be able to tolerate a larger gamma dose than 0.2 Gy/hr. The performed simulations gave a maximum gamma doses of 0.07 Gy/hr and 0.08 Gy/hr for the BWR and VVER cases, respectively. MCNP6™ code was used for the gamma dose calculations just mentioned as well as all other simulations presented in this report unless stated otherwise. The .80c cross sections were used for all calculation unless specified otherwise.

7 Discussion of Net Multiplication

In the introduction to the PNAR technique, the conceptual image of interrogating the assembly with a distributed source of low energy neutrons originating from a liner that was located less than 10 mm outside of the assembly was described. This description contains two key details about the multiplication being measured by the PNAR technique: (a) the interrogating neutrons are low in energy, from ~0.5 eV down to a thermal distribution, and (b) the interrogating neutrons are starting from the exterior of the assembly. Note, once a fission chain is started, the neutron energy becomes much higher, that of the Watt Fission Spectrum; additionally, the neutrons that multiply throughout the assembly are primarily born with energies in the MeV range, while induced fission most commonly occurs at thermal energies because the fission cross section is much larger at thermal energies.

In this section, we will compare the PNAR measurement of multiplication with the more typically discussed "net multiplication" of the assembly. The net multiplication calculation starts with a spontaneous fission source spatially distributed among all the pins in the assembly. Before comparing the PNAR Ratio with net multiplication, we will define some of the key factors involved in the calculation of the net multiplication value generated automatically by the MCNP6™ code. First the net multiplication is defined as the "average number of neutrons per source neutron." In the fuel simulation presented in this report, some of the multiplication related details are the following:

1. The neutrons are created with equal probability from any voxel in any of the UO_2 containing regions that fill the 100 pins in the 10x10 BWR assembly or the 126 pins in a VVER PWR assembly.
2. The neutrons start with an energy that is sampled from the Watt Fission Spectrum for ^{244}Cm.
3. The multiplication is impacted by the material that surrounds the assembly for the 1.2-meter section of fuel that was simulated. The central portion of the assembly has detectors around the fuel while most of the assembly is surrounded by water or PE in the case of some of the VVER simulations.
4. We decided to not use a reflecting boundary at the top and bottom of the simulated fuel section, a decision which will slightly lower the net multiplication value than if this option had been used.
5. The net multiplication values quoted in this report, except when stated otherwise, are only for the simulations made without the Cd-liner in place. This is consistent with the conceptual understanding of the PNAR technique as interrogating the high multiplying assembly with low energy neutrons, those below ~0.5 eV, that originate from the location occupied by the Cd-liner when it is present.

As part of the NGSI-SF Project [15] [16], the multiplication of several assemblies was tracked from the time before entering the reactor out to 80 years. [17] [18] This data, illustrated in Figure

6, is included here to illustrate how the multiplication of an assembly is not expected to change much once it has left the reactor, the multiplication is essentially insensitive to change after 40 years of cooling. Also, evident in Figure 6 is the difference in multiplication between the three nearly fully irradiated assemblies (green, red, blue) and the partially irradiated assembly (purple), which, given an initial enrichment of 4 wt.% and burnup of 30 GWd/tU is approximately 15 GWd/tU short of full irradiation.

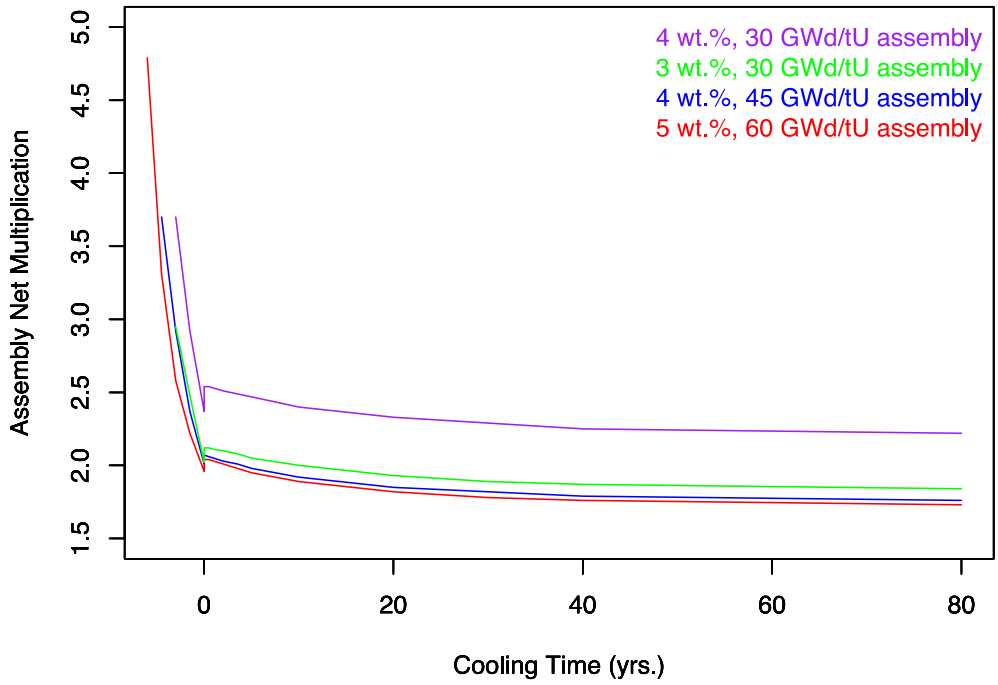

Figure 6, the estimated variation in the net multiplication of 4 different assemblies from the NGSI-SF Project spent Fuel Library 2a. [18]

8 PNAR Ratio Results – Parameter Space Exploration

In Figure 7 and Figure 8, the calculated PNAR Ratios for 12 assemblies are illustrated as a function of the initial enrichment and burnup of those assemblies; while in Table 2 and Table 3, the net multiplication, PNAR Ratio, and propagated MCNP6™ tally uncertainty for these same assemblies are listed for BWR and VVER assemblies, respectively. All the irradiated fuel assemblies illustrated in Figure 7 and Figure 8, have a cooling time of 20-years. The three assemblies in Figure 7 and in Figure 8 with PNAR Ratios of approximately 1.0 have the same isotopic composition as the data points directly above them; these three assemblies each have two data points in Figure 7 and Figure 8 because they were simulated both with and without the MCNP6™ "nonu" card, a card which will be discussed

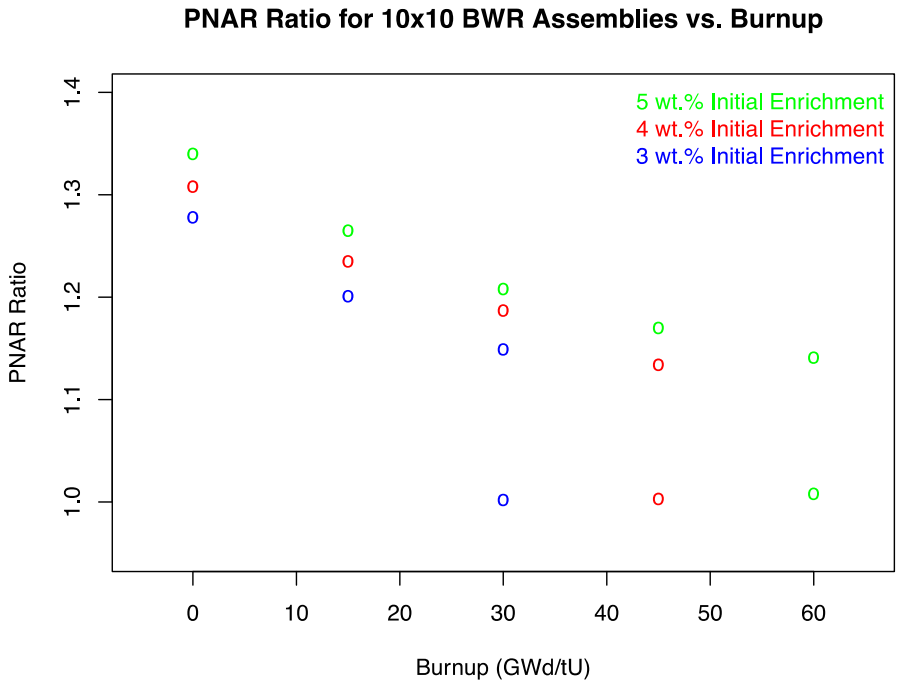

Figure 7, the BWR PNAR Ratio, simulated with fresh water, is illustrated as a function of burnup for 12 assemblies of various initial enrichments and burnup values. The cooling time is 20 years. The vertical extent of each data point is approximately equal to 4-sigma of MCNP6™ statistical uncertainty. The data graphed here is listed in Table 2. The PNAR Ratio values of ~1.0 used the nonu card.

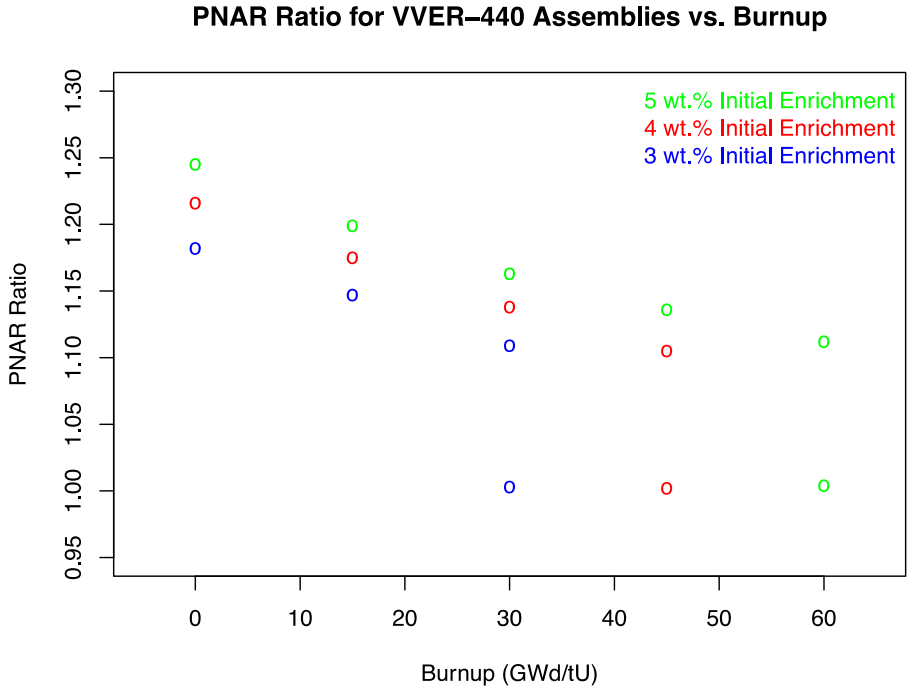

Figure 8, the VVER PNAR Ratio, simulated with borated water, is illustrated as a function of burnup for 12 assemblies of various initial enrichments and burnup values. The cooling time is 20 years. The vertical extent of each data point is approximately equal to 3-sigma of MCNP6™ statistical uncertainty. The data graphed here is listed in Table 3. The PNAR Ratio values of ~1.0 used the nonu card.

in greater detail in this section. The MCNP6™ tallied results, with their MCNP6™ estimated uncertainty, are listed in Appendix B for both BWR and VVER assemblies. Note that the MCNP6™ uncertainty represents the statistical uncertainty dependent on the number of particles run in the simulation.

To calculate the PNAR Ratio depicted in Figure 7 and Figure 8, the neutron count rates from each of the assemblies were calculated twice: once with the Cd-liner around the fuel and one without the Cd-liner. The PNAR Ratio is calculated by taking the ratio of the count rate measured for the high multiplying setup, which exists when the Cd-liner is not present, to that of the count rate when the fuel is in the low multiplying setup, which is created when the Cd-liner is inserted. Yet, since the neutron count rate is equivalent to the neutron source term multiplied by the MCNP6™ tally results, and since the neutron source term is identical in both the high and low multiplying setups, taking the ratio of the tally results directly, which give the probability of neutron detection per source particle, is equivalent to the ratio of the count rates. The isotopic mixture for the various burnup values listed for each assembly come from previous research performed by Trellue et al. [18] [19] [20]

IE (WT.%)	BURNUP (GWD/TU)	M	PNAR RATIO	ONE SIGMA PNAR RATIO (ABS., PERCENTAGE)
5*	60*	1.001	1.004	0.002, 0.20%
5	60	1.238	1.112	0.003, 0.28%
5	45	1.285	1.136	0.003, 0.29%
5	30	1.335	1.163	0.004, 0.31%
5	15	1.407	1.199	0.004, 0.33%
5	0	1.487	1.245	0.004, 0.36%
4*	45*	1.001	1.002	0.002, 0.20%
4	45	1.231	1.105	0.003, 0.27%
4	30	1.294	1.138	0.003, 0.29%
4	15	1.360	1.175	0.004, 0.32%
4	0	1.428	1.216	0.004, 0.34%
3*	30*	1.001	1.003	0.002, 0.20%
3	30	1.235	1.109	0.003, 0.27%
3	15	1.300	1.147	0.003, 0.30%
3	0	1.359	1.182	0.004, 032%

Table 2, the PNAR Ratios, net multiplications and MCNP6™ uncertainties are listed for the 12 BWR assemblies that were simulated in fresh water. Each assembly has a cooling time of 20 years. An "" indicates cases for which the "nonu" card was used.*

IE (WT.%)	BURNUP (GWD/TU)	M	PNAR RATIO	ONE SIGMA PNAR RATIO (ABS., PERCENTAGE)
5*	60*	1.001	1.004	0.002, 0.20%
5	60	1.238	1.112	0.003, 0.28%
5	45	1.285	1.136	0.003, 0.29%
5	30	1.335	1.163	0.004, 0.31%
5	15	1.407	1.199	0.004, 0.33%
5	0	1.487	1.245	0.004, 0.36%
4*	45*	1.001	1.002	0.002, 0.20%
4	45	1.231	1.105	0.003, 0.27%
4	30	1.294	1.138	0.003, 0.29%
4	15	1.360	1.175	0.004, 0.32%
4	0	1.428	1.216	0.004, 0.34%
3*	30*	1.001	1.003	0.002, 0.20%
3	30	1.235	1.109	0.003, 0.27%
3	15	1.300	1.147	0.003, 0.30%
3	0	1.359	1.182	0.004, 032%

Table 3, the PNAR Ratios, net multiplications and MCNP6™uncertainties are listed for the 12 VVER assemblies that were simulated in borated water with the detector illustrated in Figure 3 to Figure 5. Each assembly has a cooling time of 20 years. An "" indicates cases for which the "nonu" card was used.*

Three enrichment values were simulated in the creation of the assemblies illustrated in Figure 7 and Figure 8: 5.0, 4.0 and 3.0 wt.% ^{235}U. This range of initial enrichment was selected because it spans most of the initial enrichment values used in the nuclear industry. Each assembly started as a fresh assembly with the enrichment values listed; then each assembly was irradiated using the Monteburns code [18] in steps of 15 GWd/tU until they reached a level of irradiation near to the level at which they would be removed from a reactor. For this reason, there are 5 assemblies with 5 wt.% initial enrichment with burnup values of 60, 45, 30, 15 GWd/tU and fresh. There are 4 assemblies with 4 wt.% initial enrichment with burnup values of 45, 30, 15 GWd/tU and fresh. And there are 3 assemblies with 3 wt.% initial enrichment with burnup values of 30, 15 GWd/tU and fresh.

As mentioned earlier, there are three assemblies in Figure 7 and Figure 8 that were simulated in a manner different than all the other assemblies. These three assemblies are "nearly fully-irradiated" (3 wt.% 30 GWd/tU, 4 wt.% 45 GWd/tU, 5 wt.% 60 GWd/tU). Each of these assemblies was simulated in the traditional manner, for which each neutron history is run to fruition

meaning the neutron is either absorbed or leaves the depicted geometry. Then the PNAR Ratio for these three assemblies were calculated again with the inclusion of the "nonu" card. The nonu-card alters the simulation by ending any history that would normally result in an induced fission reaction. In other words, an induced fission reaction is replaced with an absorption reaction after which the history is terminated. The utility of the nonu-card is that it gives the PNAR Ratio for a non-multiplying assembly.

It is worth emphasizing that commercially produced assemblies, unlike the simulated ones used in this report such as those depicted in Figure 7 and Figure 8, are subject to the practical constraints of reactor operation. Of note in this context is the economic incentives experienced by reactor operators. The operators do not want to pay to enrich an assembly to a greater level than needed. In other words, operators want to optimally extract the potential nuclear energy inherent in each assembly.

The following are the main points noted for Figure 7, Figure 8, Table 2 and Table 3:

1. The change in the PNAR Ratio with irradiation is a smooth function of irradiation for a given initial enrichment. If an assembly starts with more potential nuclear energy by the virtue of its initial enrichment, it will be measured to have an elevated PNAR Ratio at a given burnup.
2. There is a very large separation in the measured PNAR Ratio between a fully irradiated assembly and a non-multiplying assembly; the magnitude of this separation, in terms of the PNAR Ratio, is on the same order of difference as that which exists between a fresh and a fully-irradiated assembly. **This large separation between typical assemblies and non-multiplying assemblies gives a preliminary idea of how the PNAR instrument may help detect the absence of multiplying material**. A more detailed study on the performance of PNAR given various substitution scenarios is needed, yet such research is beyond the scope of this current work. Some pin replacement research was performed by Conlin et al. [4] as part of the NGSI-SF Project. Of note from that earlier work, the PNAR Ratio was more sensitive to fuel substitution in the center of the assembly than it was on the exterior.
3. The presence of boron in the water with VVER assemblies, which was not present with the BWR assemblies, has a noticeable impact on the PNAR Ratio and the net multiplication. The PNAR Ratio changed 0.174 between a fresh and a fully irradiated 4 wt.% BWR assembly in water, and 0.111 between a fresh and a fully irradiated 4 wt.% VVER assembly in borated water. This represents a 36% smaller dynamic range due primarily to the presence of boron.

In Table 2 and Table 3 the net multiplication, which was calculated by the MCNP6™ code by following the neutrons emitted from within each assembly, is listed along with the PNAR Ratio. In Figure 9 and Figure 10 the relationship between these two variables is illustrated for the same 15 BWR and 15 VVER assemblies illustrated in Figure 7 and Figure 8.

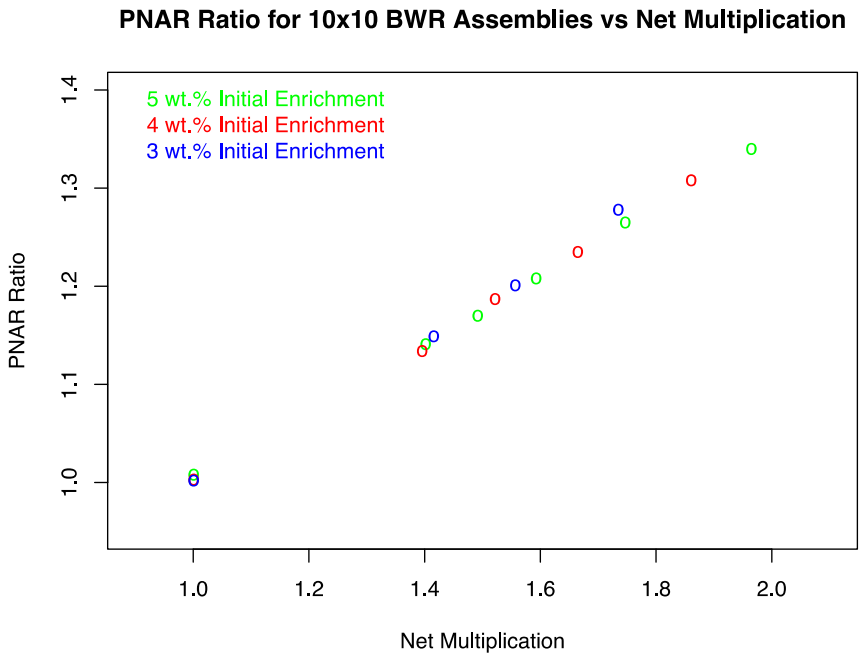

Figure 9, the PNAR Ratio is graphed as a function of the net multiplication calculated by the MCNP6 ™code for BWR assemblies in water. The three data points simulated with the nonu-card are located at approximately (1.0, 1.0); these three assemblies are isotopically identical to the three assemblies with net multiplication of approximately 1.40, because they have the same burnup. The vertical extent of each data point is approximately equal to 4-sigma of MCNP6 ™statistical uncertainty.

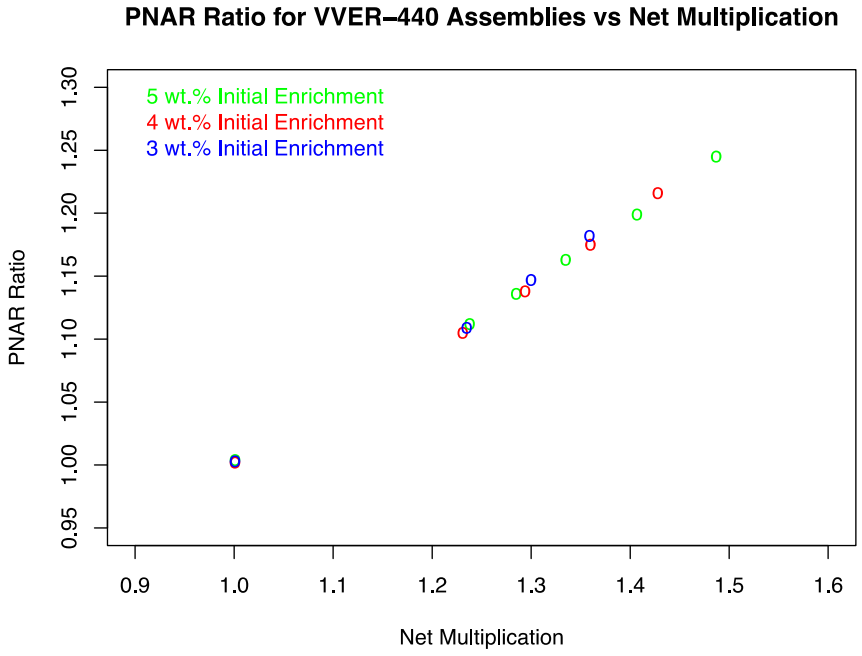

Figure 10, the PNAR Ratio is graphed as a function of the net multiplication calculated by the MCNP6 ™ code for VVER assemblies in borated water. The three data points simulated with the nonu-card are located at approximately (1.0, 1.0); these three assemblies are isotopically identical to the three assemblies with net multiplication of approximately 1.23, because they have the same burnup. The vertical extent of each data point is approximately equal to 3-sigma of MCNP6 ™statistical uncertainty.

The main point evident in both Figure 9 and Figure 10 is that **there is a smooth, nearly linear relationship between the net multiplication and the PNAR Ratio**.

9 PNAR Ratio Results – Design Options

The VVER fuel design case was different from the BWR case in that the VVER fuel is situated in a pool with boron in the water. As is evident in Figure 5, a large PE slab, the same length as the Cd-liner, was used in the VVER design to increase the multiplication in the high multiplying section. This decision also has the advantage of reducing the uncertainty of the PNAR Ratio on the variable boron content of the water, which is expected to vary from 13 to 15 g of boric acid per kg of water. Unless stated otherwise, all VVER simulations were performed with 14 g of boric acid per kg of water.

As noted in the previous section, the presence of boron in the water significantly reduces the sensitivity of PNAR. In the hope of improving the sensitivity, the possibility of using different materials beyond the Cd-liner for the high and low multiplying cases was explored. Optimizing two sections of the PNAR instrument would likely result in the need for two physically separated sections. This flexibility might allow the low multiplying section to be even lower in multiplication and/or the high multiplying section to be even higher in multiplication.

No research was performed to increase the multiplying level of the high multiplying section, because desirable materials such as beryllium were not seen as practical. As for the low multiplying section, two variations on the initial design, which was comprised of regular PE and a Cd-liner, were examined. The first design change involved replacing the regular PE block with borated water using the water that is already there; this design was motivated by simplicity and cost savings. The Cd-liner was still present. For this new design, the full set of 12 assemblies was simulated. In Figure 11 the "o" symbol represents the "original" PE containing design (identical to the data shown in Figure 10), "w" represents the design using "borated water" and Cd.

The second additional design, represented by the "p" symbol in Figure 11, involved replacing the regular PE block with "borated PE." The Cd-liner was still present. For this design, only three assemblies were simulated: (a) fresh 4 wt.%, (b) 4 wt.%, 45 GWd/tU and 20 years cooled, and (c) isotopic mixture of a 4 wt.%, 45 GWd/tU and 20 years cooled, yet, simulated with the nonu card present.

The following insights were gained from the data illustrated in Figure 11 and listed in Table 4:

1. For each of the three PNAR designs, there is a smooth nearly linear relationship between net multiplication and the PNAR Ratio.
2. Of the three designs tested, **the borated PE plus Cd-liner design provided the greatest sensitivity**. Using the original low multiplication section design, comprised of regular PE and Cd, as a reference (difference = 1.216 - 1.105 = 0.111 +/-0.005) the two other designs are the following; the uncertainties are MCNP6™ uncertainties only:
   a) The design using **borated water** reduced the sensitivity by 9% (difference = 1.099 – 1.001 = 0.098 +/-0.005) as the fuel changed from fresh 4 wt.% to fully spent (4 wt.%, 45 GWd/tU, 20 yrs cooled).

b) The design using **borated PE** increased the sensitivity by 21% (difference = 1.304 – 1.178 = 0.126 +/-0.004) as the fuel changed from fresh 4 wt.% to fully spent (4 wt.%, 45 GWd/tU, 20 yrs cooled).

In thinking about design changes such as those proposed in this section, it is important to recall that for a single location PNAR instrument, the practicality of moving mass around the assembly needs to be considered. Moving a 1 mm thick Cd-liner is considered practical while moving borated PE is not; hence, using borated PE would likely require two physically separated PNAR sections.

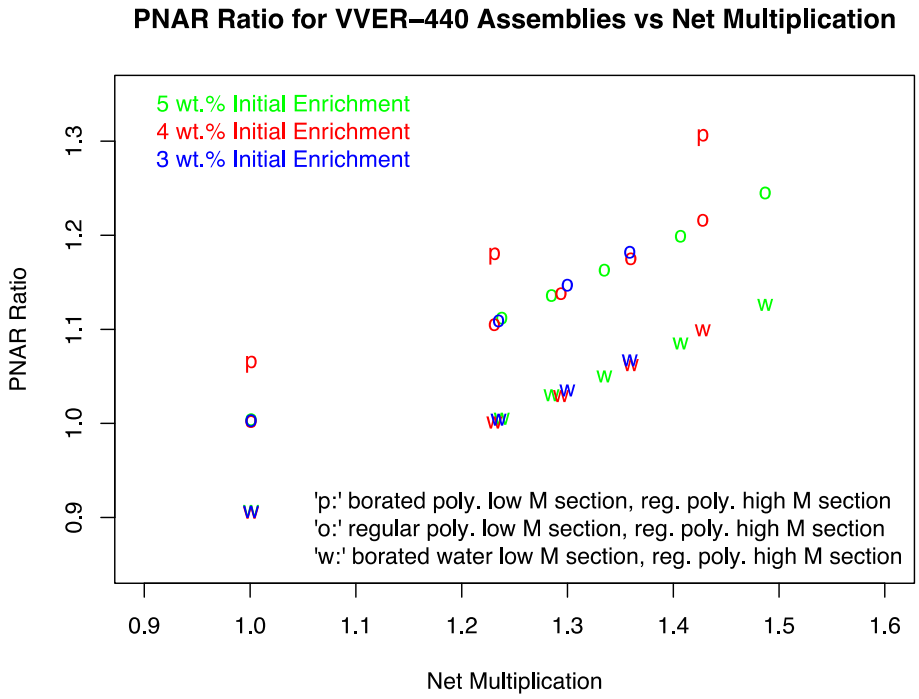

Figure 11, the relationship between the net multiplication and the PNAR Ratio is illustrated for three different PNAR designs. In all designs the high multiplying section is unchanged and the low multiplying section has a Cd-liner. The change is in the material behind the Cd-liner. The data labeled 'o' is identical to the data shown in Figure 10.

IE (WT.%)	BURNUP (GWD/TU)	M	PNAR RATIO BORATED H_2O	PNAR RATIO BORATED PE
5*	60*	1.001	0.907	
5	60	1.238	1.005	
5	45	1.285	1.030	
5	30	1.335	1.050	
5	15	1.407	1.085	
5	0	1.487	1.126	
4*	45*	1.001	0.905	1.063
4	45	1.231	1.001	1.178
4	30	1.294	1.029	
4	15	1.360	1.062	
4	0	1.428	1.099	1.304
3*	30*	1.001	0.906	
3	30	1.235	1.004	
3	15	1.300	1.035	
3	0	1.359	1.067	

Table 4, the PNAR Ratios, net multiplications are listed for the 12 VVER assemblies that were simulated in borated water. Each assembly has a cooling time of 20 years. An "" indicates cases for which the "nonu" card was used.*

10 PNAR Ratio Results – Cooling Time Dependency

Six additional assemblies were simulated to examine the impact of cooling time on the PNAR Ratio values given that all the assemblies present thus far have had 20-year cooling times. It may be that a regulator would want to use a declaration to correct for any impact of cooling time or it may be that the cooling time impact, as hinted at in Figure 6, is so little that it can be ignored. The purpose of this section is to better understand how the cooling time impacts the PNAR signal.

The additional cooling time varying assemblies were created by taking the isotopes for the three most fully irradiated assemblies listed in Table 2 and calculating what isotopes remained 40 and 80 years after discharge from the reactor. The cooling times of 40 and 80 were selected because these assemblies were previously created by the NGSI-SF Project. The fuel to be interred in the Finnish repository is expected to have a cooling time range of between 20 and 60 years but it is possible the upper limit on cooling time may extend further in time. In Table 5 and Table 6 the simulated results are listed for these three nearly fully irradiated assemblies for both BWR and VVER assemblies, respectfully. In Figure 12 and Figure 13 the PNAR Ratio is illustrated as a function of the net multiplication for all cooling times simulated for both BWR and VVER assemblies, respectively. These two figures look very much the same as Figure 9 and Figure 10. The new points added here are clustered around a net multiplication value of 1.4 in Figure 12 and 1.22 in and Figure 13.

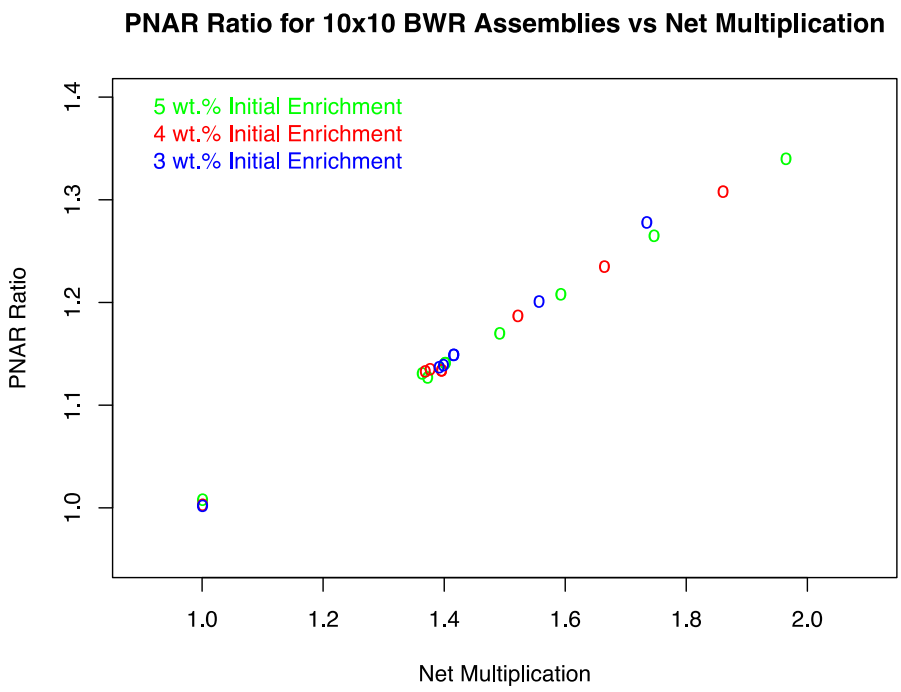

Figure 12, the BWR PNAR Ratio is graphed as a function of the net multiplication as was done in the creation of Figure 9. The difference between Figure 9 and this figure is that 3 assemblies with cooling times of 40 years and 3 assemblies with cooling times of 80 years were included. All these assemblies group around a multiplication value 1.4 and a PNAR Ratio of 1.14.

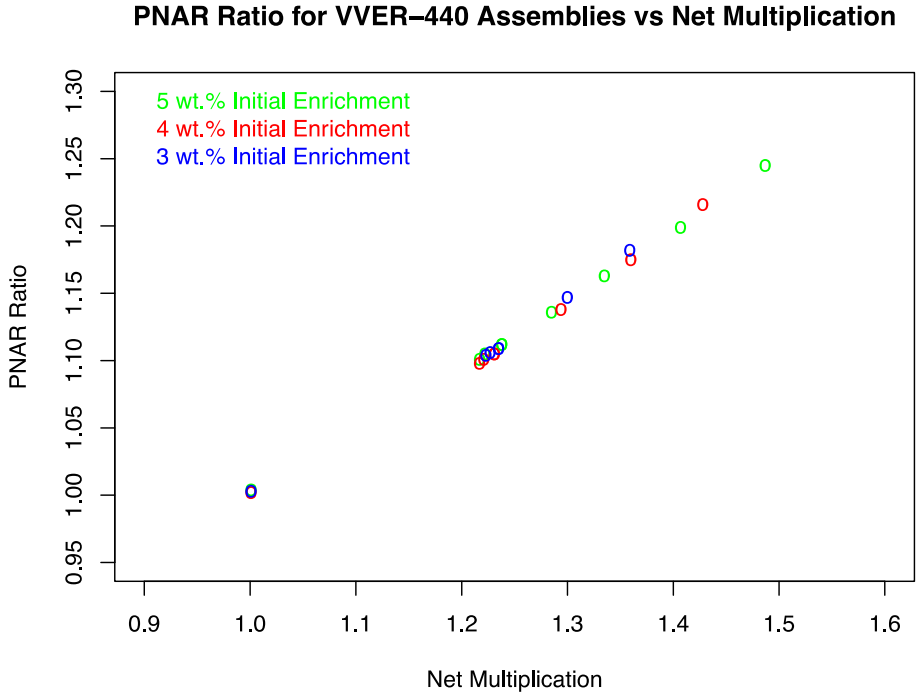

Figure 13, the VVER PNAR Ratio is graphed as a function of the net multiplication as was done in the creation of Figure 10. The difference between Figure 10 and this figure is that 3 assemblies with cooling times of 40 years and 3 assemblies with cooling times of 80 years were included. All these assemblies group around a multiplication value 1.22 and a PNAR Ratio of 1.10.

IE (WT.%)	BU (GWD/TU)	CT (YRS)	M	PNAR RATIO	ONE SIGMA (ABS., PERCENTAGE)
5	60	20	1.402	1.141	0.003, 0.30%
5	60	40	1.364	1.131	0.003, 0.30%
5	60	80	1.373	1.127	0.003, 0.29%
4	45	20	1.396	1.134	0.003, 0.30%
4	45	40	1.377	1.135	0.003, 0.30%
4	45	80	1.369	1.133	0.003, 0.29%
3	30	20	1.416	1.149	0.003, 0.30%
3	30	40	1.399	1.139	0.004, 0.31%
3	30	80	1.392	1.137	0.003, 0.30%

Table 5, variation in the PNAR Ratio as a function of cooling time for three nearly fully irradiated BWR assemblies.

BU (GWD/TU)	BORIC ACID (G)	NET M	PNAR RATIO	ONE-SIGMA (ABS., PERCENTAGE)
45	13	1.236	1.111	0.003, 0.23%
0	13	1.440	1.223	0.002, 0.17%
45	14	1.231	1.105	0.003, 0.27%
0	14	1.428	1.216	0.004, 0.34%
45	15	1.226	1.103	0.002, 0.22%
0	15	1.417	1.210	0.002, 0.16%

Table 6, variation in the PNAR Ratio as a function of cooling time for three nearly fully irradiated VVER assemblies using regular PE and Cd for the low multiplying section.

In Figure 14 and Figure 15 we have zoomed in on the cooling time dependence of the PNAR Ratio illustrated in Figure 12 and Figure 13. The data points are numbers indicating the initial enrichment of each assembly and colored to indicate the cooling time. In Table 7, the amount that the PNAR Ratio changed as the assemblies aged from 20 years to 40 years and then again from 40 years to 80 years are listed.

A good starting point for analyzing the variation in the PNAR Ratio as a function of cooling time is Figure 6, in which the cooling time variation of the net multiplication is graphed from discharge until 80 years for 4 different assemblies. What is clear from this graph is that the net multiplication doesn't change much over the time of interest to the Finnish encapsulation facility. From the data graphed in Figure 6, on average the net multiplication fell by 4.8% as the fuel aged from 20 years to 80 years. Of that reduction 3.2% of it occurred between 20 years and 40 years and 1.6%

between 40 years and 80 years. From the research of Hu et al., [21] the primary physics causing a change in multiplication as a function of time is the decay of ^{241}Pu to ^{241}Am with a 14-year half-life and the decay of ^{155}Eu to ^{155}Gd with a 4.7-year half-life. The first of these two reactions reduces the total amount of fissile material as well as increases the amount of the neutron absorber ^{241}Am, while the second reaction increases the amount of the strong neutron absorber ^{155}Gd.

The following are some of the conclusions taken away from the cooling time dependency of the PNAR Ratio performed in this section:

1. If there were a strong cooling time dependence in the PNAR Ratio measurements, we would expect the 9 data points in both Figure 14 and the 9 points in Figure 15 to exhibit a collective negative slope for a given assembly. If this were the case, the green data point for a given assembly would have a larger multiplication than the red which would then be greater than the blue. We do notice this for 3 of the 6 assemblies.
2. It is important to question the accuracy of the assemblies being simulated particularly relative to the topic being studied. It is expected that the decay of isotopes within an assembly will be accurately calculated as the relevant half-lives are well known. Yet, there is uncertainty in the starting masses of the relevant isotopes. For example, how accurately approximated is the ^{241}Pu mass or the ^{155}Eu mass in the initial simulation? The accuracy of the simulations of irradiated assemblies is a very important question for those planning on matching declarations. It is also a large question which will not be addressed in detail in this report.
3. In Table 5 and Table 6 the statistical MCNP6™ uncertainty in the PNAR Ratio is listed as 0.003. While in Table 7 the change is the PNAR Ratio over time intervals of 20 to 40 years and from 40 to 80 years are listed. Combining these two pieces of information provides a rough impression that for the level of uncertainty in the calculations, we are limited in our ability to make conclusions by the sensitivity of the simulations. As the fuel aged from 20 to 40 years in 3 of the 6 cases researched we have around a 3-sigma variation, in one case it is 2–sigma and in the remaining two cases it is around 1-sigma. Looking at the longer-term change in multiplication from 20 to 80 year there is a 2-sigma or greater change in 5 of 6 cases. Hence, the general conclusion, as was made in point 1 in this list, is that a rough cooling time dependent change is observable in the data but the real message is that what is observable will depend on the total uncertainty of the actual system. The 0.003 uncertainty in the data presented here is an MCNP6™ uncertainty of the individual data points which is dependent on the number of particles simulated.
4. We chose to study the impact of cooling time as a variable because (1) we could, given the assembly libraries we had, and (2) we thought that it might simplify future analysis if the cooling time were found to be insignificant. Yet, the most likely path forward is to follow the path set by Euratom [10] which involves a detailed simulation of the fuel irradiation, which would include the cooling time. Hence, for estimating the uncertainty of the PNAR instrument, **the uncertainty due to cooling time will be included in the overall uncertainty expected when comparing measurement to simulation**, along with other variables such a burnup, irradiation patterns, nuclear data, etc.

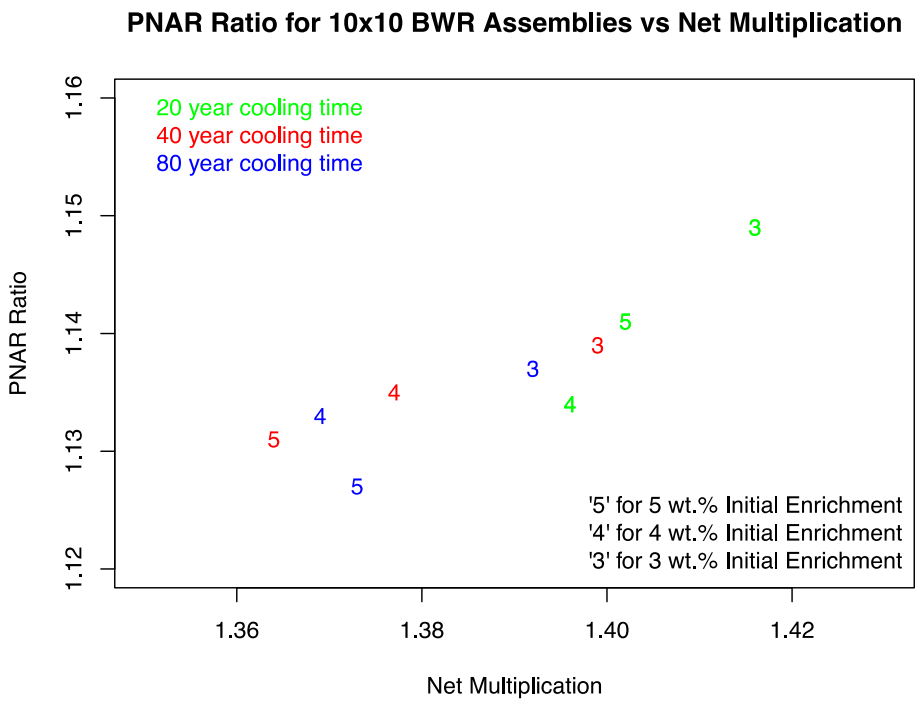

Figure 14 provides a zoomed in view of the portion of Figure 12 for which there are data points with multiple cooling times. The color of the data points indicated the cooling time while the symbol used indicated the initial enrichment.

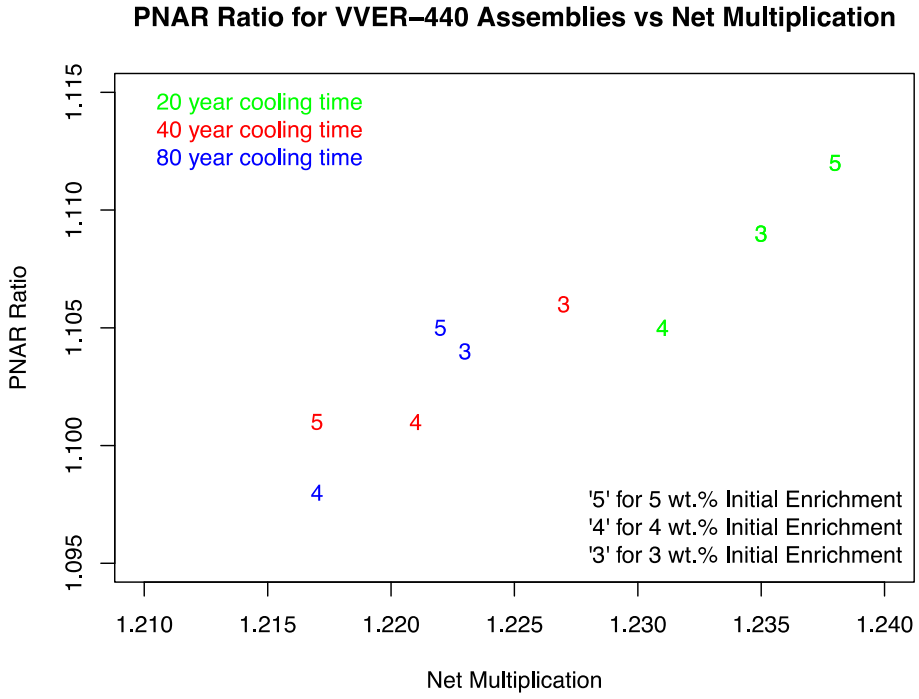

Figure 15 provides a zoomed in view of the portion of Figure 13 for which there are data points with multiple cooling times. The color of the data points indicated the cooling time while the symbol used indicated the initial enrichment.

BU (GWD/TU)	BORIC ACID (G)	NET M	PNAR RATIO	ONE-SIGMA (ABS., PERCENTAGE)
45	13	1.236	1.111	0.003, 0.23%
0	13	1.440	1.223	0.002, 0.17%
45	14	1.231	1.105	0.003, 0.27%
0	14	1.428	1.216	0.004, 0.34%
45	15	1.226	1.103	0.002, 0.22%
0	15	1.417	1.210	0.002, 0.16%

Table 7, change in the PNAR Ratio for each of the three fully irradiated assemblies simulated. The change was calculated for both BWRs and VVERs for two time intervals: 20 to 40 years and 40 to 80 years.

11 PNAR Ratio Results – Assembly Position Sensitivity

In graphs such as Figure 12 and Figure 13 the PNAR Ratio was illustrated to correlate linearly with net multiplication. How useful the PNAR technique will be in measuring multiplication will depend on the precision of each measurement as well as the overall sensitivity of the deployed instrument. As such, a focus of this report is to quantify, as best we can, each anticipated uncertainty and to identify any uncertainties not quantified. Related to this focus on quantifying the uncertainty, we need to provide information that will help select and inform the needed detection efficiency and count time so that the level of precision is consistent with the realistic accuracy of the PNAR instrument.

One of the uncertainties anticipated for a PNAR instrument is the position of the assembly inside the detector. For all the simulations discussed so far in this report, the assembly was centered in the middle of the instrument with an equal amount of water on all sides. In this section, the change in the PNAR ratio is quantified for two additional cases: (a) the assembly is positioned against one side of the detector wall with the assembly being centered along that side of the detector wall. And (b) the assembly is pushed into one corner. For each of these cases the PNAR Ratios and their uncertainties were calculated for both BWR and VVER assemblies.

Because the change in the PNAR Ratio is rather small given the detector opening anticipated for the Finnish deployment case, it was necessary to run significantly more particles relative to the simulations presented so far in this report. For this reason, a cluster at the Helsinki Institute of Physics was used in the simulations presented in this section. With this change of hardware came an associated change in software to MCNP5 V1.40 running with 0.60c cross sections. To have confidence that the change of simulation code and cross sectional data did not impact the conclusion, the following points are noted: (a) All the assemblies depicted in Figure 12 and Figure 13 were simulated with MCNP5 and MCNP6. Comparison between the two showed that there was a slight systematic shift between the two sets of codes and cross sections. (b) Note that the results for which the MCNP5 code is being used is a **comparison** of MCNP5 results with MCNP5 results, a relative change; hence, it is expected that the differences responsible for the systematic shift be-

tween the two codes will cancel out. Specifically, we are comparing the PNAR Ratio calculated when the assembly is centered in the detector to the PNAR Ratio when the assembly is against the side of as well as in the corner of the detector.

The goal of this section is to estimate a realistic uncertainty for the positioning of the assembly within the instrument. Before estimating this value from the simulations, it merits mentioning that the best manner of estimating this uncertainty is to measure multiple assemblies, multiple times, while releasing the assembly from the crane system and picking it up again between each measurement. In the absence of such an effort we have simulated two displacement cases as well as the perfectly centered case and will compare among these cases.

Given the three assembly positions that were simulated, two analysis paths are suggested for quantifying how much uncertainty is introduced. In one scenario, we assume that the assembly does not move at all between the measurement made with the Cd-liner in place as compared to the measurement made without the Cd-liner. This scenario is possibly representative of the case when the Cd-liner is moved inside the walls of the detector and the assembly is not moved between both measurements. The fact that the assembly is not moved vertically does not assure that the assembly will not move horizontally, but the likelihood of such horizontal motion is reduced. One can imagine that the assembly might be braced against one side of the detector walls thus keeping the assembly still.

Tables containing the calculated results discussed in this section are listed in Appendix C and referenced in this section. In Table 20 the PNAR Ratio for the BWR cases of (a) a centered assembly, (b) an assembly on the side and (c) an assembly in the corner for a 3 wt%, 30 GWd/tU, 20-yr cooled were listed as 1.1522, 1.1526 and 1.1529, respectively, each with an MCNP5 calculated statistical uncertainty of 0.07% or 0.0008 units of the PNAR Ratio. The mean value of these three data points is 1.1526 with a standard deviation of 0.0003 or 0.03% among the three points relative to the mean. Note that the numerical seed used to start each simulation in all the positioning simulation was different. Given that the uncertainty of each individual PNAR Ratio is greater than the standard deviation among the three data points, in addition to the inherent difficulty of performing statistical analysis on so few data points, we make the very rough estimate that we expect the positioning uncertainty of the BWR assemblies to be on the order of 0.001 units of the PNAR Ratio.

In performing the analysis of the previous paragraph, we assume that the assembly does not move at all between the measurement made with the Cd-liner in place as compared to the measurement made without the Cd-liner. In this paragraph, we will assume that the assembly is free to move between the two measurements. This data is also listed in Table 20. Hence, as an example, for the case simulated with the Cd-liner present we assume the assembly is centered while we assume that the "without the Cd-liner" simulation could be any one of the following: in the center, in the corner or against the side. In this way, we calculated 9 unique PNAR Ratio permutations, each individual value with an uncertainty of 0.07% or 0.0008: 1.1522, 1.1513, 1.1511, 1.1534, 1.1526, 1.1524, 1.1540, 1.1531, 1.1529. The mean value of these 9 points is 1.1526 with a standard deviation of 0.08% or 0.0009. As compared to the analysis performed with the assumption that the assembly did not move between the measurement of a given assembly, both approaches obtained the same mean value of 1.1526. In the analysis that allowed for the assembly to move between the two measurements of a given assembly, the one sigma uncertainty increased to be slightly

larger than the uncertainty on the individual data points. The conclusion from the analysis based on the assumption that the fuel moves between measurements and that the fuel does not move, is the same: the uncertainty due to positioning is anticipated to create an uncertainty with a one-sigma variation on the order of 0.001 units of the BWR PNAR Ratio.

Table 21 is identical to Table 20 except that a 4 wt%, 45 GWd/tU, 20-yr cooled assembly was simulated instead of a 3 wt%, 30 GWd/tU, 20-yr cooled assembly. The mean PNAR Ratio value calculated for the three assemblies that did not move between measurements were 1.1475, 1.1478 and 1.1492, each with an MCNP5 calculated statistical uncertainty of 0.07% or 0.0008 units of the PNAR Ratio. The mean value of these three data points is 1.1481 with a standard deviation 0.06% or of 0.0007 among the three points relative to the mean. For the calculation of the 9 unique PNAR Ratios permutations, each individual value with an uncertainty of 0.07%, the values are the following: 1.1475, 1.1473, 1.1472, 1.1480, 1.1478, 1.1477, 1.1494, 1.1492, 1.1492. The mean value of these 9 points is 1.1481 with a standard deviation of 0.07% or 0.0008. As with the analysis presented in the previous paragraph, the conclusions from the simulations performed with the 4 wt%, 45 GWd/tU, 20-yr cooled BWR assembly is that **the uncertainty due to positioning of BWR assemblies is anticipated to create an uncertainty with a one-sigma variation on the order of 0.001 units of the PNAR Ratio.**

The same calculations described in the previous several paragraphs were performed for VVER assemblies using 3 wt%, 30 GWd/tU, 20-yr cooled and 4 wt%, 45 GWd/tU, 20-yr cooled assemblies. The calculated values are listed in Table 24 and Table 25. The conclusion for the VVER assemblies is like that of the BWR assemblies but slightly larger in magnitude. For the 3 wt.% case, the PNAR Ratio was calculated to be 1.1129 +/- 0.0007 from the scatter among the three cases that assume the assembly did not move during a PNAR measurement. The PNAR Ratio was calculated to be 1.1129 +/- 0.0011 when the 9-possible permutation were considered. For the 4 wt.% case, the PNAR Ratio was calculated to be 1.1129 +/- 0.0016 from the scatter among the three cases that assume the assembly did not move during a PNAR measurement. The PNAR Ratio was calculated to be 1.1129 +/- 0.0014 when the 9-possible permutations were considered. In all the simulations presented in this section the uncertainty of any individual PNAR Ratio is close to that of the uncertainty calculated from the scatter among the PNAR Ratios. Hence, the conclusions of this section are rough. But the uncertainties are small. **The main conclusion for the VVER assemblies is that the uncertainty due to positioning is anticipated to create an uncertainty with a one sigma variation on the order of 0.002 units of the PNAR Ratio.**

12 PNAR Ratio Results – Boron Variability in the Water

Because the VVER assemblies in Finland are stored in a pool with water that is borated, and boron is a good absorber of neutrons, the impact of variation in the boron content needs to be researched. It is anticipated that the boron content is monitored for safety reasons; however, it is not clear that such measurements could be used to correct the PNAR signal to account for any variation in the boron content. It is assumed for the purposes of this report that a measure of boron will not be used to correct measurements but rather that the boron content is bound between "known" extremes.

BU (GWD/TU)	BORIC ACID (G)	NET M	PNAR RATIO	ONE-SIGMA (ABS., PERCENTAGE)
45	13	1.236	1.111	0.003, 0.23%
0	13	1.440	1.223	0.002, 0.17%
45	14	1.231	1.105	0.003, 0.27%
0	14	1.428	1.216	0.004, 0.34%
45	15	1.226	1.103	0.002, 0.22%
0	15	1.417	1.210	0.002, 0.16%

Table 8, variation in the PNAR Ratio as a function of boron content in the water in units of grams of boric acid per kg of fresh water. Two VVER assemblies were simulated: 4 wt.%, 45 GWd/tU, 20 years cooled, and a fresh 4wt.% assembly.

From the facility operators, we learned that the boric acid in the pool can vary between 13 and 15 g per kg of fresh water. For this reason, all the VVER results in this report, except some results presented in this section, were simulated with 14 g of boric acid per kg of water. In this section, the PNAR ratios are given for two cases: (a) a 4 wt%, 45 GWd/tU, 20-yr cooled assembly and (b) a fresh 4 wt.% assembly. For these two cases, the boric acid content was set to 13, 14 and 15 g boric acid per kg of water. In Table 8 the simulated results are listed. Recall that the net multiplication is the multiplication calculated when the fuel is in the high multiplying section of the detector; this calculation also includes the 0.23 m of the assembly that extends beyond the top and bottom of the detector. The PNAR Ratio uncertainty is listed as a percentage of the PNAR Ratio and as an absolute value. The uncertainty of the net multiplication is on the order of 0.01% or less.

In Table 8 the PNAR Ratios are listed for the 6 cases described. To put these simulations into a practical context, it is assumed that during calibration of the system, the boron content is measured accurately and, for simplicity's sake, is assumed to be 14 g per kg of water. Under this scenario, the first analysis step is to see how much the PNAR Ratio changes when the boric acid content drops to 13 g per kg of water or increases to 15 g. The 13 and 15 g cases were run longer than the 14 g cases to reduce the error on the end points of this range so that an estimate of the change per gram could be more accurately estimated. For the fresh fuel case the change is 0.007 +/- 0.003/gram, while for the fully spent fuel case the change was 0.004 +/- 0.004/gram. It is thought that the fresh fuel is more sensitive to changes in the boron content because it is significantly more multiplying than the fully spent fuel. Additionally, the clear majority of the fuel to be measured at the encapsulation facility will be fully irradiated; hence, the change in the PNAR Ratio due to the boron variation of 0.004 +/- 0.004/gram is taken to be the more representative value to use if the boron variation is to be treated as an uncertainty in the PNAR Ratio.

The variability of the boron content gives the facility or state a knob that it can turn to change the NDA results, not only the PNAR results but the total neutron results. As such, we anticipate that the IAEA and Euratom will want some verified measure of the boron content. Yet, as stated previously, the use of such a measurement to perform a “boron content correction” is not clear. In the absence of such a decision/understanding, the subjective decision is made here to include **the variation in the boron content as an uncertainty of 0.005 for the VVER assemblies.**

13 Counting Statistics

There is considerable variability in terms of what count rate the neutron detectors can have. It is possible to change the detection material (^{3}He, boron, ^{235}U), the amount of moderator, the detector size, gas pressure, the use of Cd around the detector unit, etc. In the current study, we started with a ^{3}He tube because, from the start, we knew that a short measurement time was a priority. From simulations and literature, we expect the boron lined tubes to be ~8 times less efficient than equivalently sized ^{3}He tubes [22] [23], while we expect fission chambers to be roughly 1,000 times less efficient than equivalently sized ^{3}He tubes. In Appendix D issues related to counting statistics are described in detail. The key points from that Appendix are summarized here:

- The ratio of the neutron emission rate of the strongest assembly expected to be measured to the weakest assembly is approximately 225. Both the strong burnup dependence and the cooling time dependence of this ratio were quantified in producing this estimate. Both the (α,n) and spontaneous fission neutron sources were included in the estimate of the source strength.
- If the PNAR detector is designed to measure the strongest intensity assembly at the highest count rate recommended for the ^{3}He tube and associated electronics, then the following PNAR Ratio can be expected for a fully irradiated assembly. The values listed here are from Table 34 and represent the statistic when two separate 2-minute counting intervals are used for a PNAR measurement:
  - Lowest emission assembly: 1.134 **+/- 0.005**
  - Typical emission assembly: 1.134 **+/- 0.001**
  - Strongest emission assembly: 1.1343 **+/- 0.0003**

Note, the PNAR Ratio values listed above are all the same value because the multiplication of the assemblies in all three cases is assumed to be about the same as they are for a fully irradiated assembly. Such fully irradiated assemblies will likely fall in some range, for example from 1.125 to 1.145; the PNAR Ratio value is not what is of interest in this list, it is the uncertainty. What is changing in each assembly that causes the statistics to change is the neutron source term. Based on the neutron emission rate, the lowest emitting case is anticipated to have an emission rate representative of a 17 GWd/tU, 60 years cooled assembly; the typical emission case is representative of a 32 GWd/tU, 40 years cooled assembly; while the strongest assembly is representative of a 55 GWd/tU, 20 years cooled assembly.

14 Absolute Count Rates

The most intense assembly from a neutron source strength perspective being designed for in Finland is a 55 GWd/tU, 20-year cooled assembly. From the NGSI-SF Spent Fuel Library 2a we expect a 60 GWd/tU, 5 wt.% ^{235}U, 20-year cooled assembly 17x17 PWR to emit ~2.5e8 n/s. Taking into consideration that our simulations only include 1.2 meters of the fuel and the difference in mass per unit length of a 17x17 PWR and a 10x10 BWR, the emission rate appropriate for a 1.2 meter section of a 60 GWd/tU, 10x10 assembly is 2.5e7 n/s. Assuming that the neutron emission varies as the burnup to the 4th power, we expect the 55 GWd/tU assembly to emit 30% fewer neutrons than a 60 GWd/tU assembly; hence we estimate the 1.2-meter section of the most intense 10x10 BWR to emit 1.8e7 n/s.

As noted in Table 12, the neutron detection probability of four 0.2 m active length, 17.4 mm diameter, 6 atm pressure ^{3}He tube is expected to be 3.72e-3 counts per source particle for a 60 GWd/tU, 5 wt.%, 20 year cooled BWR assembly when the Cd-liner is not in place (assembly #2 is Tables 14 and 15). Hence, for a 10x10 BWR assembly that emits 1.8e7 n/s in a PNAR instrument that detects 3.72e-3 counts per source particle, we expect a count rate of around 6.7e4 counts/s or 1.7e4 counts/s per tube.

Per the recommendations of Nathan Johnson of GE Reuter-Stokes, the single 0.2 m active length tube specified here has an upper count rate limit of 5e4 counts/s, a limit for which a 5% dead-time is anticipated. Thus, **the current BWR PNAR design is close to the maximum anticipated count rate but is low by a factor of ~3.0**. Per tube the count rate is a factor of 12 below the limit specified by Nathan Johnson.

Repeating the above calculation for the VVER assembly, the 1.2-meter section of the most intense VVER assembly (55 GWd/tU, 20 years cooled) is expected to emit 1.9e7 n/s; note that the emission rates for the VVER and BWR are about the same because the VVER only has 3% greater mass per unit length even though the VVER has 126 pins as compared to the 100 pins for the BWR; the shorter pellet radius in the case of the VVER reduces the pellet mass per unit length. Note that the BWR emission intensity is expected to vary as a factor of axial length; in this study, an average BWR neutron intensity value was used that is nearly the same as the PWR value. [24] Additionally, unless the details of a precise irradiation are known, particularly with BWR assemblies (void ratio, absorber blade insertion, etc.), the emission from a given burnup can vary over a significant range. As a result, the values used here are rough and anticipated to be valid within about a factor of 2.

As noted in Table 17 the neutron detection probability of six 0.1 m active length, 17.4 mm diameter, 6 atm pressure ^{3}He tube is expected to be 2.05e-3 counts per source neutron for a 60 GWd/tU, 5 wt.%, 20 year cooled VVER assembly when the Cd-liner is not in place (assembly #2 is Tables 16 and 17). Hence, for a VVER-440 assembly that emits 1.9e7 n/s in a PNAR instrument that detects 2.05e-3 counts per source particle, we expect a count rate of around 3.9e4 counts/s or 6.5E3 counts/s per tube. This count rate for the system of 4 tubes is ~5 times below the maximum count rate used in the analysis in Appendix D. Note that the count rate for an individual tube is a factor of 31 below that recommended by Nathan Johnson.

Key points in the context of the absolute count rate:

1. The limit recommended by Reuter-Stokes is not a solid limit. It is the value expected to produce about a 5% dead-time. Dead-time corrections are reliable at more elevated values than 5%; yet, it does not appear that investigation in this direction are needed given that the individual tubes in the currently designed systems are factors of 12 and 31 below the count rates that would produce a 5% dead-time.
2. Because detailed irradiation simulations were not made of the assemblies of interest, particularly of the BWR assemblies, the neutron intensities of interest are anticipated to be accurate to within approximately a factor of 2. As with the previous bullet, this uncertainty is not expected to be of concern given that the currently designed systems are far from count rates of concern
3. Changes to (a) the PE thickness around the ^{3}He tube, (b) the tube diameter, (c) the tube length or (d) the number of tubes could be considered if elevating the count rate is desirable.

4. Until the uncertainty of the system is known, the acceptable uncertainty in the counting statistics is not known. In the subsequent sections, we will revisit the absolute count rate in the context of the system uncertainty.

15 Cumulative Uncertainties

The discussion of the cumulative uncertainty of the BWR and VVER-440 PNAR instruments designed for the Finnish Encapsulation Facilities combines a range of factors. Some of these factors can be approximated through simulation more easily than others. Additionally, some of the relevant uncertainty factors are embedded in how the PNAR instrument is to be used. The major relevant factors are discussed in the following list:

1. **Uncertainty due to location of the assembly in the detector opening**: The one-sigma uncertainty of moving an assembly around in the PNAR instrument for the tube arrangement detailed in this report (BWR: four, 0.2 m long ^{3}He tubes, VVER: six, 0.1 m long ^{3}He tubes) with tubes located on all sides of the assembly was quantified as the following:
   a) BWR: 0.001
   b) VVER: 0.002
   Recall that a proper quantification of this uncertainty should be obtained by measuring a few assemblies multiple times.
2. **Uncertainty due to variation in the boron content of the water**: The boron content is expected to vary between 13 and 15 g per kg of water for the VVER assemblies only. If the system can be calibrated at the mid-point of this variation and if no correction is made based on measurements of the boron content, then **a one-sigma uncertainty of 0.005 in the PNAR Ratio is anticipated when measuring VVER-440 assemblies**.
3. **Uncertainty due to anisotropy of the assembly burnup**: For the simulations performed in this study, all the pins were taken to have experienced the same burnup and to have started with the same initial enrichment. The use of poison rods was not considered. It is not clear how much uncertainty should be attributed to this condition.
   a) It is noted that the burnup among typical commercial pins varies on the level of 20% from the most irradiated pin to the least irradiated pin. It is not known to the author if burnable poisons, when the assembly is irradiated to fruition, alter this general observation.
   b) One option would be to lump the anisotropy of irradiation uncertainty into the uncertainty of simulating the irradiation of the assembly in the reactor given that one of the primary purposes of these NDA measurements is to verify the declaration. For this declaration verification, the assembly must be simulated and anisotropy can possibly be handled at that time, to the degree that the needed data is available.
   c) Additional relevant points in this context include the following:
      i. The positioning of ^{3}He detectors on all sides of the assembly minimizes the anticipated inaccuracy of heterogeneous burnup as the measured signal will be averaged over all sides evenly.
      ii. **Multiplication as a process that naturally averages over the assembly.** The PNAR detectors are lined with Cd to be sensitive to only the higher energy neutrons leaving the fuel; causing the signal to be originating from deeper in the assembly. Additionally, the multiplication process involves neutrons being born generally at the MeV energy levels, slowing down 8 orders of magnitude, inducing fission in the thermal energy range, before the process begins again; **this chain reaction process**

means that the measured multiplication inherently interrogates a wide volume of the assembly; this is inherent to the reason the Cd-liner needs to be ~0.5 meter in the vertical direction.

The effort involved in simulating the wide range of irradiation scenarios necessary to capture the variation that exists among commercial fuel and then to propagate the neutrons from those assemblies to the PNAR detectors is well beyond the resources of this current study. In the absence of this research, we do not have a satisfactory value for the uncertainty caused by the anisotropy of the fuel. To make a **very rough estimate**, we note that the PNAR Ratio changes by 0.05 as a 4 wt.% BWR assembly in water is irradiated from 30 to 45 GWd/tU; additionally, the PNAR Ratio changes by 0.03 as a 4 wt.% VVER assembly in borated water is irradiated from 30 to 45 GWd/tU. We expect that the change caused by ~18-months of irradiation will create a change in the measured multiplication that is much larger than that caused by the anisotropy of the isotopes among the pins. If we assume the anisotropy causes an uncertainty that is 10% of the change caused by ~18-months of irradiation we obtain the following:

a) BWR: 0.005
b) VVER: 0.003

4. **Uncertainty due to cooling time**: What is clear from the simulations performed in this report is that the uncertainty caused by ignoring the cooling time is small as a function of cooling time; **this is an unique property relative to the other measured NDA signatures; the multiplication is expected to change by ~5% over the time window of interest, 20 to 60 years, while all other signatures are expected to change by ~60% or more**. Cooling time is also a declared quantity so the small uncertainty due to cooling time can be included in the simulation of the fuel irradiation and subsequent isotopic decay while the assemblies remain outside the reactor.
5. Uncertainty due to all the cumulative uncertainties involved in accurately simulating the irradiation of assemblies while in the reactor as well as simulating the neutron transport within the PNAR instrument. The uncertainty inherent in the simulation of spent fuel is a widely-researched topic and is beyond the scope of this work. This topic is included in this list because it will impact the accuracy and uncertainty of the calibration of the PNAR instrument. The uncertainty in the simulations will depend heavily on (a) the quality of the information provided, and (b) the specific quantity estimated. Will only safeguards data be used? Or will reactor operator data with void ratios and control blade insertions be included? Furthermore, some quantities like ^{137}Cs, are a direct fission product, which are more accurately estimated than the ^{244}Cm content which depends on a complex chain of multiply neutron absorptions. Because the uncertainty of reactor core operation is not considered part of the PNAR instrument or experimental setup, it is not included in the current calculation.
6. **Uncertainty due to the counting statistics**: Provided ^{3}He tubes are used, it is expected that the uncertainty due to counting statistics can remain of the same magnitude or less than the total uncertainties of the instrument. In Appendix D and summarized earlier in this study, we described that an instrument designed to count 200,000 counts/s as a system (50,000 count/s per BWR tube or 33,000 counts/s per VVER tube) for the strongest intensity assembly expected (55 GWd/tU, 20 years cooled) at the Finnish Encapsulations Facility would produce the following results for a fully irradiated assembly given 2-minutes for each of the two PNAR measurements:
    i. Lowest emission assembly: 1.134 **+/- 0.005**
    ii. Typical emission assembly: 1.134 **+/- 0.001**

iii. Strongest emission assembly: 1.1343 **+/- 0.0003**

A typical assembly is a 32 GWd/tU, 40 years cooled assembly and the weakest assembly is 17 GWd/tU, 60 years cooled assembly. In later sections, we calculated that the conceptual instruments designed for this study were 3 and 5 times less efficient than the ideal case. Below we list the uncertainty due to counting statistics alone for the systems as designed for a 2-minute measurement with each PNAR section:

a) BWR design used in this report:
   i. Lowest emission assembly: 1.134 +/- 0.009
   ii. Typical emission assembly: 1.134 +/- 0.002
   iii. Strongest emission assembly: 1.134 +/- 0.001

b) VVER design used in this report:
   i. Lowest emission assembly: 1.134 +/- 0.011
   ii. Typical emission assembly: 1.134 +/- 0.003
   iii. Strongest emission assembly: 1.134 +/- 0.001

If the uncertainties listed in this section are combined for a typical assembly using the quadrature sum, **the aggregate BWR uncertainty is 0.005; while the VVER uncertainty is 0.007**. Summarizing the uncertainties included in this calculation, for BWR assemblies:

- 0.005 value for anisotropy of the isotopic distribution in the fuel
- 0.001 for positioning uncertainty
- 0.002 for counting statistics

For the VVER-440 assembly the uncertainties are the following:

- 0.003 value for anisotropy of the isotopic distribution
- 0.002 for positioning
- 0.005 for variation in the boron content
- 0.003 for counting statistics.

If the 2-minute count time is not increased for the lowest emission assemblies, then the aggregated BWR uncertainty would increase to 0.010; while, for the lowest emission VVER assemblies, the uncertainty would increase to 0.013. If the count time for these lowest emission assemblies were increased to 8 minutes for each PNAR measurement, the aggregate uncertainty of the BWR case would drop to 0.007 while the aggregate uncertainty of the VVER case would drop to 0.008.

16 PNAR Sensitivity

Now that an approximate uncertainty for both the BWR and VVER-440 PNAR systems exist, we will revisit the variation in the PNAR Ratio with changes in initial enrichment, burnup and cooling time to examine how sensitive the PNAR instrument is anticipated to be. In Figure 12 and Table 2 and 5 the relevant BWR data is available and in Figure 13 and Table 3 and 6 the VVER-440 data is available. In Table 9 the change in the PNAR Ratio is listed in terms of the PNAR Ratio values as well as in terms of the number of 1-sigma variations this range represents. This calculation was made for the four assemblies most characteristic of the fuel to be entered in Finland. The PNAR Ratio variation was quantified for three different ranges: (a) For the case when the fuel transitions from fresh to fully irradiated; in the case of 3 wt.% fuel, fully irradiated means 30 GWd/tU;

while in the case of 4 wt.%, it means 45 GWd/tU. As noted before, these fully irradiated burnups are very approximate, (b) for the case of the final 15 GWd/tU of burnup, and (c) for the scenario of a fully irradiated assembly being replaced with a non-multiplying assembly.

	FROM FRESH TO FULLY IRRADIATED	**CHANGE DURING LAST CYCLE**	**FROM FULLY IRRADIATED TO NON-MULTIPLYING**
3 WT.% BWR	1.278 TO 1.149, 26-SIGMA	1.201 TO 1.149, 10-SIGMA	1.149 TO 1.002, 29-SIGMA
4 WT.% BWR	1.308 TO 1.134, 35-SIGMA	1.187 TO 1.134, 11-SIGMA	1.134 TO 1.003, 35-SIGMA
3 WT.% VVER	1.182 TO 1.109, 10-SIGMA	1.147 TO 1.109, 5-SIGMA	1.109 TO 1.003, 17-SIGMA
4 WT.% VVER	1.216 TO 1.105, 16-SIGMA	1.138 TO 1.105, 5-SIGMA	1.105 TO 1.002, 15-SIGMA

Table 9, variation in the PNAR Ratio between two different state points in absolute terms and in terms of the number of sigma for 4 different assemblies. The state points selected are (a) comparing a fresh assembly to a fully irradiated one, (b) comparing a given assembly over the last full 15 GWd/tU of irradiation, and (c) comparing a fully irradiated assembly to a non-multiplying assembly of the same isotopic composition.

The primary conclusion from this section is that both the BWR and VVER PNAR instruments, as conceptually designed, are sensitive to changes in the multiplication such that a change of 1.4 GWd/tU of irradiation for a BWR assembly and 2.9 GWd/tU of irradiation for a VVER assembly corresponds to a 1-sigma effect on the PNAR Ratio. As such, **both designs are expected to be adequate to verify that the measured assembly is multiplying at the level expected based on the declaration.** The BWR instrument is about twice as sensitive as the VVER instrument. The primary reason for this is the reduced dynamic range of the VVER system due to boron in the water. Furthermore, **for the VVER system, the less sensitive system, approximately a 15-sigma change in the PNAR Ratio is expected if a fully irradiated assembly were replaced with a non-multiplying assembly in the expected borated water environment**.

17 PNAR Deployment Options

There are a variety of physical options for measuring an assembly in a high and low multiplying setup. For the current Finnish situation, there are two primary options and both have ramifications on uncertainty:

1. The assembly and the neutron detectors could remain static and a movable Cd-liner could be moved in and out of the region where the detectors are located. The Cd-liner would move during the time interval between the two PNAR measurements.
2. Two different sets of detectors could be deployed, one set in a high multiplying section and one set in a low multiplying section. The assembly would move between the two PNAR measurements so that the same section of the fuel could be measured in each section. The Cd-liner would be built into the wall of the low multiplying section of PNAR.

The advantage of moving the Cd-liner is that it reduces the number of neutron detectors by a factor of two. It also should reduce the positioning uncertainty of the fuel given that the fuel is not

intentionally moved between the two measurements. Additionally, moving the Cd-liner allows both the high and low multiplying section measurements to be completed during the PGET measurement time.

The primary positive attribute of moving the assembly between different PNAR sections is the lower probability of an NDA system failure given that only passive parts would be used. The facility crane would be used to move the fuel between PNAR sections.

A negative attribute in the context of moving Cd is that the motion of the Cd creates moving parts, which increases the probability of mechanical failure/maintenance. The negative with moving the assembly between section is that such a move would increase the measurement time in the context of sharing time with the PGET instrument and likely increase the cost provided that the duplicate detector system costs more than the system needed to move the Cd-liner. An additional cost increase resulting from the presence of two detector sections is that the support structure will become larger.

18 Cadmium-Liner Thickness

For all the simulations presented to this point in this report, the Cd thickness was 1.0 mm. For most NDA neutron systems used in the safeguards profession, the Cd thickness used is either 0.5 or 1.0 mm. To test the impact of varying the Cd thickness, two VVER and two BWR assemblies were simulated for four different Cd-liner thickness so that the change in the dynamic range as a function of Cd-liner thickness could be examined. The results are listed in Table 10 for which the assemblies were a fresh 4 wt.% assembly and a 4 wt.%, 45 GWd/tU, 20-year cooled assembly. Note that the low multiplying section used for this Cd-liner thickness research was not the same as illustrated in Figure 5 for which PE formed the slabs surrounding the assembly. Instead the slabs contained borated water; this difference is not expected to alter the conclusions related to the Cd-liner thickness.

From the data in Table 10, a gradual increase in the dynamic range of the PNAR Ratio is noted as the Cd thickness increases, roughly a 5% change in the dynamic range is observed as the Cd thickness is increased 8-fold from 0.25 mm to 2.0 mm. It is recommended that 0.5 mm be used in any deployment. The thickness of 0.25 mm is expected to be easy to tear, while working with 0.5 mm has worked well per the experience of the authors.

	0.25 MM THICK Cd-LINER	0.5 MM THICK Cd-LINER	1.0 MM THICK Cd-LINER	2.0 MM THICK Cd-LINER
BWR, 0 - 45 GWD/TU	1.284 TO 1.115 DELTA: 0.169	1.296 TO 1.123 DELTA: 0.173	1.308 TO 1.134 DELTA: 0.174	1.323 TO 1.146 DELTA: 0.177
VVER, 0 - 45 GWD/TU	1.087 TO 0.991 DELTA: 0.096	1.094 TO 0.994 DELTA: 0.099	1.099 TO 1.001 DELTA: 0.098	1.111 TO 1.010 DELTA: 0.102

Table 10, variation in the PNAR Ratio between two different state points in absolute terms for both BWR and VVER instruments. The two state points selected are a fresh 4 wt.% assembly and a 4 wt.%, 45 GWd/tU, 20-year cooled assembly.

A few additional points of note in the context of the Cd-liner:

1. If a thickness of 0.5 mm is used and all the neutron detectors are on one level, it is expected that the Cd liner length can be reduced by 0.14 m to 0.6 m. For such a length, the Cd mass will be 1.6 kg.
2. It is desirable to keep the Cd as close as reasonably possible to the fuel.
3. It is highly desirable to minimize the amount of water between the Cd and the fuel; and if there is some, it is extremely important that the thickness of the water layer be constant for each assembly.
4. The structure involved in moving the Cd up and down will require the detectors to move back away from the fuel relative to the conceptual design in the report, which did not allocate room for hardware needed to move the Cd. It is desirable that the detectors be as close as reasonably possible to the fuel.
5. The liner needs to move at a speed of ~1 meter per minute or faster. This is driven by the need to finish the PNAR measurement in under 5 minutes. Hence, two minutes measuring one PNAR section, one minute moving the Cd-liner, then two minutes measuring the second PNAR section is the suggested scenario.
6. Given that a future PNAR instrument may measure over 10,000 assemblies, it is worth approximating how much of the ^{133}Cd, the main absorbing isotope in the liner, might be depleted. Given that ^{133}Cd is 12% of the Cd mass, there is a total of 200 g or 1.7 moles or 1e24 atoms of ^{133}Cd. Recall that we expect the most intense assembly to emit ~1e7 n/s. If we assume that the liner absorbs all the neutrons emitted and that all the assemblies are as intense as the most intense assembly and that we are measuring 24 hours a day every day, we calculate that it would take 1e15 s to deplete 1% of the ^{133}Cd from the liner. This is much longer than a century so there is no concern regarding depleting a 0.5 mm thick Cd-liner.

19 Cadmium-Liner Length

The neutron simulations in this report followed neutrons in a volume that was 0.8 m by 0.8 m by 1.2 meters. The assembly was centered in the horizontal cross-section; the longest direction was the axial direction. The plane between the two detector layers bisected the assembly in two even halves. The Cd-liner extended 0.37 m above and below this mid-plane for a total vertical extent of 0.74 m. Thus, there was a 0.23-meter extent of fuel above and below the Cd-liner for which there

was no Cd-liner. To examine how close the Cd-liner was to its optimal length, the PNAR Ratio was calculated for both fresh 4 wt.% and 4 wt.%, 45 GWd/tU, 20-year cooled assemblies for both BWR and VVER fuel when the Cd-liner length was extended by 0.23 m above and below the 0.74 m liner, creating a 1.2 m length Cd-liner. In the case of the BWR assemblies, the dynamic range was increased from 0.174 to 0.177 for a total change of 1.4%. For the VVER assemblies the same change in the Cd-liner resulted in the dynamic range changing from 0.0983 to 0.0988 for a change of 0.6%; as with the Cd thickness studies, the slabs outside the assembly were filled with borated water. The BWR assembly was impacted more than the VVER assembly due to the elevated multiplication of the BWR assembly. The neutron chain reaction events, which contribute to the PNAR signal, travel over a larger volume when neutrons in the setup multiply more; hence, the impact of the Cd-liner length is more pronounced with BWR assemblies.

The primary conclusion from these results is that **the Cd-liner can be shortened in the final design** for two reasons: (a) if the detectors are located on one vertical level, this would reduce the Cd-liner by ~0.10 meter, (b) given the results discussed in this section, we expect that the Cd-liner can be reduced by another ~0.10 meter without significantly reducing the dynamic range, particularly for the BWR design, where we arguably have more dynamic range than we need to assure the inspectorates that the assembly is multiplying at the level expected for the declared fuel.

20 Water Gap around the Fuel

To examine the impact of a change in the water gap around the fuel, the case of doubling the water gap with a fresh 4 wt.% and 4 wt.%, 45 GWd/tU, 20-year cooled assemblies for both BWR and VVER fuel was simulated. For the BWR setup the dynamic range changed from 0.174 units to 0.150 units for a sensitivity reduction of 14%. For the VVER setup the dynamic range changed from 0.098 units to 0.071 units for a sensitivity reduction of 28%. The greater sensitivity of the VVER design to additional water is consistent with previous observations that the presence of borated water is particularly detrimental to the PNAR technique because it lowers the overall multiplication and it limits the ability of the Cd liner to alter the multiplication; hence, reducing the ability of the instrument designer to create two sections of significantly different levels of multiplication.

It is worth emphasizing that **if the detector is fabricated properly, the water gap should not change during operation**. Yet, in the design phase of the instrument, the water gap is a design variable.

There are two main points to note in the context of the water gap around the assembly:

1. It is desirable to keep the water gap around the fuel as small as possible. In general, this gap is the same width as the gap used in spent fuel storage containers. The gap width and the material in the gap (air, water or borated water) determine how sensitive the instrument will be to the gap width; for example, a gap of air is insignificant, water is significant and borated water is the most significant. Selecting the water gap directly impacts the dynamic range of the instrument so if the gap is to be increased one must make sure the instrument has the sensitivity needed.
2. It is important in designing the instrument to not let the water gap be variable from one assembly to the next. Practically this translates to making sure the sides of the instrument are

solid and that the motion of the Cd is a reproducible movement so that each assembly has the same water gap between the Cd-liner and the fuel.

21 Preliminary Air Design

Future NDA encapsulation needs in Finland may involve air measurements. To give some preliminary idea whether the PNAR technique will work well enough in air, the VVER design was used to examine a few initial designs. The VVER design was selected because it has, as noted in Figure 5, 0.74 m axially long poly slabs surrounding the fuel. Pictures of the setup used to simulate the air model are not shown here because the design is identical to the design illustrated in Figure 3 to Figure 5 with two exception: (1) any cell with water was replaced with air and (2) the material in the large slabs located outside the fuel, which were filled with PE in the simulations presented earlier in this report, were filled with different materials in different simulations as listed in Table 11.

The slabs in which the materials were changed are each 50 mm thick. Four different cases were simulated. In all cases PE was maintained in the section near the fuel to assure a large flux of low energy neutrons. Iron, lead and PE were each used in the middle section while only iron and lead were used in the outer section. The results are listed in Table 11.

Near section	Middle section	Far section	Dynamic range
Polyethylene	Iron	Iron	0.133
Polyethylene	Lead	Lead	0.135
Polyethylene	Polyethylene	Iron	0.127
Polyethylene	Polyethylene	Lead	0.127

Table 11, results for PNAR simulation in air with VVER setup depicted in Figure 5. The term "near, middle and far" indicated the sections' location relative to the fuel in Figure 5. The dynamic range was calculated for the change in the PNAR Ratio between a fresh 4 wt.% assembly and a 4wt.%, 45 GWD/tU, 20-year cooled assembly.

Main points for the air design:

1. **The air design** using 50 mm of PE followed by 100 mm of metal improved the **dynamic range from 0.111 to 0.133 for a 20% improvement over the borated water results**. A fresh 4 wt.% assembly and a 4wt.%, 45 GWD/tU, 20-year cooled assembly were simulated for this calculation.
2. It is expected that metal in the middle section improves the design relative to PE because any neutrons thermalizing in the middle section will have a very low probability of returning to the fuel; absorption in the PE is expected to have a high likelihood. Yet, iron or lead in the middle section have a greater probability of reflecting non-thermal neutrons back into the PE layer closest to the fuel. However, the metal in the middle section only improved the dynamic range by ~6%, so 50 mm of PE alone is likely sufficient for the air design.

22 Discussion of Some Final Design Features

In this section, a list of options with recommendations is given along with some discussion of the rationale:

1. **A circular detector cross section is recommended** because (a) the PNAR physics is improved by positioning less Cd close to the fuel in the high multiplying section, (2) the overall weight of the detector is reduced and (3) the fabrication of round objects is standard practice for fabrication facilities.
2. **A ^{3}He detector tube is recommended** rather than a boron tube or fission chamber. The greater efficiency of ^{3}He is important given the short measurement time and precision needs of the PNAR analysis. Furthermore, the additional weight for shielding is not an issue given that portability is not a requirement of this instrument. The ^{3}He tube should have the following characteristics: (a) carbon lined, (b) N_2 quench gas because the other standard options are not stable to the anticipated gamma dose and (3) aluminum walls to minimize the electron flux into the gas from gamma interactions. A 17.4 or 25.4 mm diameter tube filled to a pressure of 6 atm is recommended.
3. It is suggested that data acquisition software be designed so that the count time used is automated to always reach the chosen uncertainty.
4. Issue yet to be resolved:
   c) **Currently the Cd-liner is 0.74 meters long.** Given recent results indicating that additional Cd did not improve the PNAR sensitivity significantly, the 0.74 m length can be shortened but exactly how much needs to be determined via further study.
   d) It may be desirable to include **additional 3He tubes** for redundancy or to give the IAEA independent detectors.
   e) It is currently assumed that the uncertainty variation due to change in the boron content will simply be accepted as an uncertainty. **If the boron content were measured**, this uncertainty could be reduced.

23 Conclusions

In this report, the performance of two conceptual PNAR instruments was described, one for BWR assemblies and one for VVER-440 assemblies. Both conceptual designs satisfied the primary safeguards purpose of the instruments, which is to verify that a given assembly was multiplying at the level expected. Of note in this regard, a 35-sigma difference between a non-multiplying assembly and a fully irradiated assembly was calculated for the BWR instrument, while for the VVER assembly there was a 15-sigma difference between these same two cases. Furthermore, the inclusion of the PNAR instrument, along with the PGET instrument, produced an NDA system that satisfies all the recommendation of the IAEA ASTOR Group of Experts. Hence, a PNAR instrument has the capability to significantly improve the safeguards system by detecting the removal of a significant amount of multiplying material. This performance was achieved with hardware that is less complex, less expensive than the other NDA techniques generally considered for the measurement of multiplication; in fact, the hardware is not much more complex than that of a Fork detector. [25] **The building of a prototype is highly encouraged.**

References

[1] D.M. Lee and L.O. Lindqvist, "Self-Interrogation of Spent Fuel," Los Alamos, LA-9494-MS, UC-15, 1982.

[2] H.O. Menlove and D.H. Beddingfield, "Passive Neutron Reactivity Measurement Technique," LA-UR-97-2651, Los Alamos, 1997.

[3] S.J Tobin and et. al., "Non-Proliferation Technology Development Study for UREX," International Atomic Energy Agency Symposium on International Safeguards: Addressing Verification Challenges, 2006.

[4] J.L. Conlin, S.J. Tobin, J. Hu, T.H. Lee, H.O. Menlove, "Passive Neutron Albedo Reactivity with Fission Chambers," LA-UR-11-00521, 2010.

[5] A. Bolind, "Development of an Analytical Theory to Describe the PNAR and CIPN Nondestructive Assay Techniques," *Annals of Nuclear Energy*, vol. 66, pp. 167-176, 2014.

[6] T. Honkamaa, F. Levai, A. Turunen, R. Berndt, S. Vaccaro and P. Schwalbach, "A Prototype for Passive Gamma Emission Tomography," *Symposium on International Safeguards: Linking Strategy, Implementation and People, Vienna, Austria,* 2014.

[7] SCALE: "A Comprehensive Modeling and Simulation Suite for Nuclear Safety Analysis and Design," Oak Ridge National Laboratory, Oak Ridge, TN, ORNL/TM-2005/39, June 2011.

[8] T. Goorley et al., "Initial MCNP6 Release Overview," *Nuclear Technology,* vol. 180, pp. 298-315, Dec. 2012.

[9] ASTOR Group Report 2011-2016, "Technologies Potentially Useful for Safeguarding Geological Repositories," *International Atomic Energy Agency, STR-384, Vienna, Austria* 2017.

[10] S. Vaccaro, J. Hu, J. Svedkauskaite, A. Smejkal, P. Schwalbach, P. De-Baere and I.C. Gauld, "A New Approach to Fork Measurements Data Analysis by RADAR-CRISP and ORIGEN Integration," *IEEE Transactions on Nuclear Science,* vol. 61, no. 4, pp. 2161-2168, March 2014.

[11] B.D. Murphy and I.C. Gauld, "Spent Fuel Decay Heat Measurements Performed at the Swedish Central Interim Storage Facility," *U.S. Nuclear Regulatory Commission*, NUREG/CR-6971, ORNL/TM-2008/016, 2009.

[12] D. Coucill and T. Totev, "Development of a New VVER-400 Fuel Design," *British Nuclear Fuels plc. Fuel Business Group*, Springfields, Salwick, Preston.

[13] D.H. Beddingfield, N.H. Johnson and H.O. Menlove, "^{3}He Neutron Proportional Counter Performance in High Gamma-Ray Dose Environments," *Nuclear Instruments & Methods in Physics Research, Section A,* vol. 455, pp. 670-682, 2000.

[14] D. Beddingfield, H.O. Menlove and N.H. Johnson, "Neutron Proportional Counter Design for High Gamma-Ray Environments," *Nuclear Instruments & Methods in Physics Research, Section A,* vol. 422, pp. 35-40, 1999.

[15] M.A. Humphrey, S.J Tobin and K. Veal, "The Next Generation Safeguards Initiative's Spent Fuel Nondestructive Assay Project," *Journal of Nuclear Material Management,* vol. 3:XL, 2012.

[16] S.J. Tobin et al., "Experimental and Analytical Plans for the Non-Destructive Assay System of the Swedish Encapsulation and Repository Facilities," *Symposium on International Safeguards: Linking Strategy, Implementation and People,* Vienna, Austria, Vols. IAEA-CN-220-238, 2014.

[17] S.J. Tobin, M.L. Fugate, H.R Trellue, T. Burr, P. De-Baere, P. Jansson, P. Schwalbach, A. Sjoland and S. Vaccaro, "Research into Measured and Simulated Nondestructive Assay Data to

Address the Spent Fuel Assay Needs of Nuclear Repositories," in *Institute of Nulear Material Management*, Atlanta, GA, 2016.

[18] H.R. Trellue, M.L. Fensin, J.R. Richard, and J.L. Conlin, "Description of the Spent Nuclear Fuel Used in the Next Generation Safeguards Initiative to Determine Plutonium Mass in Spent Fuel," *Los Alamos National Laboratory*, LA-UR 11-00300, 2011.

[19] J.D. Galloway, H.R. Trellue, M.L. Fensin and B.L. Broadhead, "Design and description of the NGSI Spent Fuel Library with Emphasis on the Passive Gamma Signal," *Journal of Nuclear Material Management,* vol. 3:XL, 2012.

[20] R.A Weldon, M.L. Fensin and H.R. Trellue, "Total Neutron Emission Generation and Characterization for a Next Generation Safeguards Initiative Spent Fuel Library," *Progress in Nuclear Energy,* vol. 80, pp. 45-73, 2015.

[21] J. Hu, S.J. Tobin, H.O. Menlove, S. Croft, M.T. Swinhoe, M.L. Fensin, T.H. Lee and J.L. Conlin, "Assessment of the Californium Interrogation Prompt Neutron (CIPN) Technique for the Next Generation Safeguards Initiative Spent Fuel Research Effort," *Los Alamos National Laboratory*, LA-UR11-06890, 2011.

[22] R.D. McElroy and S. Croft, "Application of 10B-Lined Proportional Counter to Traditional Neutron Counting Application in International Safeguards," *Oak Ridge National Laboratory Report*.

[23] Z. Wang and C.L. Morris, "Multi-Layer Boron Thin-Film Detectors for Neutrons," *2010 Symposium on Radiation Measurements and Applications*, Ann Arbor, 2010.

[24] J. Hu, I.C. Gauld, J.L. Peterson and S.M. Bowman, "US Commercial Spent Nuclear Fuel Assembly Characteristics: 1968-2013," NUREG/CR-7227 ORNL/TM-2015/619, Oak Ridge, 2016.

[25] A. Tiitta et al., "Investigation of the Possibility to Use Fork Detector for Partial Defect Verification of Spent LWR Fuel Assemblies," ISSN 0785-9325, ISBN 951-712-590-9, Helsinki, 2002.

[26] C. Willman, "Application of Gamma Ray Spectroscopy of Spent Nuclear for Safeguards and Encapsulation," *Ph.D. Dissertation Uppsala University,* Vols. ISSN 1651-6214, no. ISBN 91-554-6637-0, 2006.

[27] P. Jansson, "Studies of Nuclear Fuel by Means of Nuclear Spectroscopic Methods," *Comprehensive Summaries of Uppsala Dissertations from the Faculty of Science and Technology,* Vols. ISSN 1104-232X, no. ISBN 91-554-5315-5. 39, 2002.

Appendix A: Passive Gamma Results

As mentioned in the main section of the paper, the reason for simulating the gamma dose received by the ^{3}He tubes was to calculate the amount of lead needed in the design to reduce the gamma dose to the tubes to an acceptable level. Because gamma rays travel further in water than neutrons, the vertical extent of the fuel was increased from 1.2 meter to 1.8 meters for the gamma simulations.

The ^{3}He tubes in the PNAR detector need to tolerate the gamma dose produced by the highest gamma intensity assembly. The most intense assembly in the context of the Finnish encapsulation facility is expected to have a burnup of ~55 GWd/tU and a cooling time of 20 years. Based upon the assembly libraries of the NGSI-SF Project [18] [19] [20] such an assembly is expected to emit ~5 x 10^{14} photons/s distributed over all the pins. This value was calculated using the isotopic masses from the 45 and 60 GWd/tU, 20-year cooled cases. The fact that the photon intensity varies approximately linearly with burnup [26] [27] for all the fuel of interest to the Finnish encapsulation facility was used. Additionally, the photon intensity calculation took into consideration the mass difference between the NGSI-SF Project assemblies relative to a 10x10 SVEA BWR assembly and a VVER-440 assembly by adjusting the intensity per unit mass.

The 662 keV photons from ^{137}Cs, 30-year half-life, account for more than ~95% of all the photons emitted from assemblies that were irradiated to a burnup of ~25 GWd/tU or more and which were cooled for more than 20 years. The next two most significant photon emitting isotopes are ^{134}Cs and ^{154}Eu. Given the short half-life, 2.6 years, and relatively moderate energy of the photons emitted by ^{134}Cs, photons from ^{134}Cs are not expected to have a significant impact on the dose to the tubes. Yet, given the elevated photon energy emitted from ^{154}Eu, 1274 keV in particular, it is important to include photons from ^{154}Eu in designing the shielded system as attenuation effectively filters for these elevated energy photons. In Table 12 the photons simulated for the 55 GWd/tU, 20 year cooled, BWR assembly setup are listed.

Isotope	Energy (keV)	Relative Intensity
^{137}CS	662	98.1%
^{154}EU	1,274	0.9%
^{154}EU	1,004	0.5%
^{154}EU	996	0.3%
^{154}EU	873	0.3%

Table 12, relative intensity of the photons emitted from both the 10x10 SVEA BWR assembly and the VVER-440 assembly for calculating the gamma dose to ^{3}He tubes. Both assemblies were irradiated to 55 GWd/tU and cooled for 20 years.

For the design illustrated in Figure 1 and Figure 2, the photon dose was calculated to be 0.07 Gy/hr or 7.0 rad/hr, while for the designs in Figure 3 to Figure 5 the photons dose was calculated to be 0.084 Gy/hr or 8.4 rad/hr. For the BWR design, most of the photons producing this dose crossed primarily through three lead surfaces in route to the ^{3}He tube: (a) the front surface closest to the assembly and (b) the top and bottom surfaces visible in Figure 1. The photon flux through the back side and the two ends of the detector were significantly less than the dose passing through the other three sides. In Table 13, the dose to the tube that passed through the different surfaces of the lead block, along with the total dose, are listed. An F4, cell flux, tally was used to calculate the dose and to track which lead surface each photon traversed. The ANSI/ANS6.1.1.11977 flux-to-dose conversion factors were used with log-log interpolation.

Surface	Dose (Gy/hr)	Dose (rad/h	DOSE Uncertainty
FRONT	0.029	2.9	1.6%
TOP AND BOTTOM	0.038	3.8	1.4%
FURTHEST (BACK)	0.0029	0.29	3.6%
BOTH ENDS	0.0002	0.02	18%
TOTAL	0.070	7.0	1.0%

Table 13, dose to one, 0.2-m long, 6 atm ^{3}He, 17.4 mm diameter tube positioned within the BWR geometry depicted in Figure 1 and Figure 2 given the incident spectrum from the most intense spent fuel assembly anticipated.

Appendix B: MCNP6™ Tally Results

In Table 14 and Table 15 the following information is listed for BWR assemblies: initial enrichment (IE) burnup (BU), cooling time, the presence or not of a 0.74 m long Cd-liner, and the direct MCNP6™ net multiplication and output tallies with MCNP6™ calculated uncertainties. The ^{3}He tube tallies were subdivided into units that were 40 mm long in the axial direction of the tube.
In Table 16 and Table 17 the following information is listed for VVER assemblies: initial enrichment (IE) burnup (BU), cooling time, the presence or not of a 0.74 m long Cd-liner, and the direct MCNP6™ net multiplication and output tallies with MCNP6™ calculated uncertainties. The ^{3}He tube tallies were subdivided into units that were 20 mm long in the axial direction of the tube.

Assembly Number	IE ^{235}U (.wt%)	Burnup (GWd/tU)	CT (years)	Cd-liner	Net M	Uncert. Net M
1	5	60	20	with	1.182	0.01%
2	5	60	20	without	1.238	0.01%
3	5	45	20	with	1.214	0.01%
4	5	45	20	without	1.285	0.01%
5	5	30	20	with	1.248	0.01%
6	5	30	20	without	1.335	0.01%
7	5	15	20	with	1.295	0.01%
8	5	15	20	without	1.407	0.01%
9	5	0	20	with	1.344	0.01%
10	5	0	20	without	1.487	0.01%
11	4	45	20	with	1.177	0.01%
12	4	45	20	without	1.231	0.01%
13	4	30	20	with	1.221	0.01%
14	4	30	20	without	1.294	0.01%
15	4	15	20	with	1.264	0.01%
16	4	15	20	without	1.360	0.01%
17	4	0	20	with	1.306	0.01%
18	4	0	20	without	1.428	0.01%
19	3	30	20	with	1.180	0.01%
20	3	30	20	without	1.235	0.01%
21	3	15	20	with	1.225	0.01%

22	3	15	20	without	1.300	0.01%
23	3	0	20	with	1.262	0.01%
24	3	0	20	without	1.359	0.01%
25	5	60	40	with	1.168	0.01%
26	5	60	40	without	1.217	0.01%
27	5	60	80	with	1.171	0.01%
28	5	60	80	without	1.222	0.01%
29	4	45	40	with	1.171	0.01%
30	4	45	40	without	1.221	0.01%
31	4	45	80	with	1.168	0.01%
32	4	45	80	without	1.217	0.01%
33	3	30	40	with	1.175	0.01%
34	3	30	40	without	1.227	0.01%
35	3	30	80	with	1.172	0.01%
36	3	30	80	without	1.223	0.01%
37*	5	60	20	with	1.001	0.00%
38*	5	60	20	without	1.001	0.00%
39*	4	45	20	with	1.001	0.00%
40*	4	45	20	without	1.001	0.00%
41*	3	30	20	with	1.001	0.00%
42*	3	30	20	without	1.001	0.00%

Table 14, MCNP6 ™output for BWR simulations performed with the geometry illustrated in Figure 1 and Figure 2. Two tables (Table 14 and Table 15) are used to present this data because of the number of columns. The high multiplying section was calculated with the 1.2 m of the assembly in the detector, in water. The low multiplying section is the same as the high multiplying section except with the addition of 0.74 m of Cd.

* “nonu card” used in simulation, fission events turned into neutron capture.

Assembly Number	IE ^{235}U (.wt%)	Burnup (GWd/tU)	CT (years)	Cd-liner	Net M	Uncert. Net M
1	5	60	20	with	1.182	0.01%
2	5	60	20	without	1.238	0.01%
3	5	45	20	with	1.214	0.01%
4	5	45	20	without	1.285	0.01%
5	5	30	20	with	1.248	0.01%
6	5	30	20	without	1.335	0.01%
7	5	15	20	with	1.295	0.01%
8	5	15	20	without	1.407	0.01%
9	5	0	20	with	1.344	0.01%
10	5	0	20	without	1.487	0.01%
11	4	45	20	with	1.177	0.01%
12	4	45	20	without	1.231	0.01%
13	4	30	20	with	1.221	0.01%
14	4	30	20	without	1.294	0.01%
15	4	15	20	with	1.264	0.01%
16	4	15	20	without	1.360	0.01%
17	4	0	20	with	1.306	0.01%
18	4	0	20	without	1.428	0.01%
19	3	30	20	with	1.180	0.01%
20	3	30	20	without	1.235	0.01%
21	3	15	20	with	1.225	0.01%
22	3	15	20	without	1.300	0.01%
23	3	0	20	with	1.262	0.01%
24	3	0	20	without	1.359	0.01%
25	5	60	40	with	1.168	0.01%
26	5	60	40	without	1.217	0.01%

27	5	60	80	with	1.171	0.01%
28	5	60	80	without	1.222	0.01%
29	4	45	40	with	1.171	0.01%
30	4	45	40	without	1.221	0.01%
31	4	45	80	with	1.168	0.01%
32	4	45	80	without	1.217	0.01%
33	3	30	40	with	1.175	0.01%
34	3	30	40	without	1.227	0.01%
35	3	30	80	with	1.172	0.01%
36	3	30	80	without	1.223	0.01%
37*	5	60	20	with	1.001	0.00%
38*	5	60	20	without	1.001	0.00%
39*	4	45	20	with	1.001	0.00%
40*	4	45	20	without	1.001	0.00%
41*	3	30	20	with	1.001	0.00%
42*	3	30	20	without	1.001	0.00%

Table 15, MCNP6™ tally results for BWR simulations performed with the geometry illustrated in Figure 1 and Figure 2. Two tables (Table 14 and Table 15) are used to present this data because of the number of columns. The high multiplying section was calculated with the 1.2 m of the assembly in the detector, in water. The low multiplying section is the same as the high multiplying section except with the addition of 0.74 m of Cd. The tally results are the average of 4 tubes.

* "nonu card" used in simulation, fission events turned into neutron capture.

Assembly Number	IE ^{235}U (.wt%)	Burnup (GWd/tU)	CT (years)	Cd-liner	Net M	Uncert. Net M
1	5	60	20	with	1.182	0.01%
2	5	60	20	without	1.238	0.01%
3	*5*	*45*	*20*	*with*	*1.214*	*0.01%*
4	5	45	20	without	1.285	0.01%
5	5	30	20	with	1.248	0.01%
6	5	30	20	without	1.335	0.01%
7	5	15	20	with	1.295	0.01%
8	5	15	20	without	1.407	0.01%
9	5	0	20	with	1.344	0.01%
10	5	0	20	without	1.487	0.01%
11	4	45	20	with	1.177	0.01%
12	4	45	20	without	1.231	0.01%
13	4	30	20	with	1.221	0.01%
14	4	30	20	without	1.294	0.01%
15	4	15	20	with	1.264	0.01%
16	4	15	20	without	1.360	0.01%
17	4	0	20	with	1.306	0.01%
18	4	0	20	without	1.428	0.01%
19	3	30	20	with	1.180	0.01%
20	3	30	20	without	1.235	0.01%
21	3	15	20	with	1.225	0.01%
22	3	15	20	without	1.300	0.01%
23	3	0	20	with	1.262	0.01%
24	3	0	20	without	1.359	0.01%
25	5	60	40	with	1.168	0.01%
26	5	60	40	without	1.217	0.01%
27	5	60	80	with	1.171	0.01%

28	5	60	80	without	1.222	0.01%
29	4	45	40	with	1.171	0.01%
30	4	45	40	without	1.221	0.01%
31	4	45	80	with	1.168	0.01%
32	4	45	80	without	1.217	0.01%
33	3	30	40	with	1.175	0.01%
34	3	30	40	without	1.227	0.01%
35	3	30	80	with	1.172	0.01%
36	3	30	80	without	1.223	0.01%
37*	5	60	20	with	1.001	0.00%
38*	5	60	20	without	1.001	0.00%
39*	4	45	20	with	1.001	0.00%
40*	4	45	20	without	1.001	0.00%
41*	3	30	20	with	1.001	0.00%
42*	3	30	20	without	1.001	0.00%

Table 16, MCNP6™ tally results for VVER simulations performed with the geometry illustrated in Figure 3 to Figure 5. Two tables (Table 16 and Table 17) are used to present this data because of the number of columns. The high multiplying section was calculated with the 1.2 m of the assembly in the detector, in borated water with a large block of PE outside the assembly as illustrated in Figure 5. The low multiplying section is the same as the high multiplying section except with the addition of 0.74 m of Cd.

* "nonu card" used in simulation, fission events turned into neutron capture.

Assem-bly Number	20 mm Tube Length	Uncert. 20 mm Tube	60 mm Tube Length	Uncert. 60 mm Tube	0.1 m Tube Length	Uncert. 0.1 m Tube
1	3.66E-04	0.56%	1.09E-03	0.37%	1.84E-03	0.30%
2	4.06E-04	0.43%	1.21E-03	0.28%	2.05E-03	0.23%
3	3.82E-04	0.55%	1.13E-03	0.36%	1.92E-03	0.29%
4	4.34E-04	0.42%	1.29E-03	0.28%	2.18E-03	0.22%
5	3.98E-04	0.55%	1.18E-03	0.36%	2.00E-03	0.29%
6	4.61E-04	0.43%	1.37E-03	0.28%	2.32E-03	0.23%
7	4.17E-04	0.53%	1.25E-03	0.35%	2.12E-03	0.28%
8	5.04E-04	0.42%	1.50E-03	0.27%	2.54E-03	0.22%
9	4.46E-04	0.42%	1.33E-03	0.28%	2.25E-03	0.22%
10	5.58E-04	0.30%	1.66E-03	0.20%	2.80E-03	0.16%
11	3.66E-04	0.56%	1.08E-03	0.37%	1.83E-03	0.29%
12	4.02E-04	0.44%	1.20E-03	0.29%	2.03E-03	0.23%
13	3.85E-04	0.55%	1.14E-03	0.36%	1.94E-03	0.29%
14	4.41E-04	0.45%	1.30E-03	0.29%	2.20E-03	0.23%
15	4.07E-04	0.54%	1.21E-03	0.35%	2.04E-03	0.28%
16	4.79E-04	0.41%	1.42E-03	0.27%	2.40E-03	0.21%
17	4.31E-04	0.42%	1.28E-03	0.28%	2.16E-03	0.22%
18	5.21E-04	0.31%	1.55E-03	0.20%	2.63E-03	0.16%
19	3.65E-04	0.57%	1.09E-03	0.37%	1.84E-03	0.30%
20	4.04E-04	0.46%	1.20E-03	0.30%	2.04E-03	0.24%
21	3.86E-04	0.54%	1.15E-03	0.35%	1.94E-03	0.28%
22	4.44E-04	0.42%	1.32E-03	0.28%	2.23E-03	0.22%
23	4.08E-04	0.43%	1.21E-03	0.28%	2.05E-03	0.22%
24	4.82E-04	0.32%	1.43E-03	0.21%	2.43E-03	0.17%
25	3.59E-04	0.56%	1.07E-03	0.37%	1.81E-03	0.29%
26	3.96E-04	0.45%	1.17E-03	0.29%	1.99E-03	0.23%
27	3.61E-04	0.55%	1.07E-03	0.36%	1.82E-03	0.29%

28	3.99E-04	0.45%	1.19E-03	0.29%	2.01E-03	0.23%
29	3.63E-04	0.55%	1.07E-03	0.36%	1.82E-03	0.29%
30	3.97E-04	0.45%	1.18E-03	0.29%	2.00E-03	0.23%
31	3.61E-04	0.56%	1.07E-03	0.37%	1.81E-03	0.29%
32	3.95E-04	0.44%	1.18E-03	0.29%	1.99E-03	0.23%
33	3.62E-04	0.57%	1.08E-03	0.37%	1.83E-03	0.30%
34	4.01E-04	0.46%	1.19E-03	0.30%	2.02E-03	0.24%
35	3.61E-04	0.57%	1.07E-03	0.37%	1.82E-03	0.30%
36	3.98E-04	0.46%	1.18E-03	0.30%	2.01E-03	0.24%
37*	2.84E-04	0.49%	8.42E-04	0.32%	1.42E-03	0.25%
38*	2.85E-04	0.45%	8.45E-04	0.30%	1.43E-03	0.24%
39*	2.85E-04	0.55%	8.45E-04	0.36%	1.43E-03	0.29%
40*	2.85E-04	0.45%	8.46E-04	0.30%	1.43E-03	0.24%
41*	2.83E-04	0.58%	8.42E-04	0.38%	1.43E-03	0.30%
42*	2.84E-04	0.47%	8.43E-04	0.31%	1.43E-03	0.25%

Table 17, MCNP6 ™output for VVER simulations performed with the geometry illustrated in Figure 3 to Figure 5. Two tables (Table 16 and Table 17) are used to present this data because of the number of columns. The high multiplying section was calculated with the 1.2 m of the assembly in the detector, in borated water with a large block of PE outside the assembly as illustrated in Figure 5. The low multiplying section is the same as the high multiplying section except with the addition of 0.74 m of Cd. The tally results are the average of 6 tubes.

* "nonu card" used in simulation, fission events turned into neutron capture.

Appendix C: Positioning Uncertainty

The purpose of this appendix is to present the results for the research focused on quantifying the change in the PNAR Ratio when the assembly moved around inside the detector. In Table 18 the detection probability for neutron when a 3 wt.%, 30 GWd/tU, 20-yr cooled BWR assembly was simulated in 6 different situations. For the first row the assembly is centered in the instrument with 5 mm of water between the assembly and the walls of the detector on all sides; a Cd-liner is in place. In the second row the Cd-liner has been removed. For the third row the assembly was pushed against one of the side walls of the detector but the assembly was centered on this wall. As such, there is no water outside the BWR box on one side of the assembly while on the opposite side there is 10 mm of water; on the other two sides, there is 5 mm of water. The fourth row is identical to the 3rd with the exception that the Cd-liner is not present. For the final two rows the assembly is situated in the corner of the detector; the fifth-row simulation has a Cd-liner while the sixth doesn't.

X-offset (mm)	Y-offset (mm)	Cd Liner	Detection Probability	MCNP5 Uncer. 1-sigma
0	0	YES	3.357E-03	0.05%
0	0	NO	3.868E-03	0.05%
5	0	YES	3.354E-03	0.05%
5	0	NO	3.865E-03	0.05%
5	5	YES	3.352E-03	0.05%
5	5	NO	3.865E-03	0.05%

Table 18, neutron detection probability for a 3 wt.%, 30 GWd/tU, 20-years cooled BWR assembly measured in the PNAR instrument for 6 different situations. The assembly was in 3 different physical locations. In each of those locations the detection probability was simulated with or without a Cd-liner present.

Table 9 is identical to Table 18 except that the simulations were performed with the isotopic mixture representative of a 4 wt.%, 45 GWd/tU, 20-yr cooled BWR assembly.

X-offset (mm)	Y-offset (mm)	Cd Liner	Detection Probability	MCNP5 Uncer. 1-sigma
0	0	YES	3.319E-03	0.05%
0	0	NO	3.809E-03	0.05%
5	0	YES	3.318E-03	0.05%
5	0	NO	3.808E-03	0.05%
5	5	YES	3.314E-03	0.05%
5	5	NO	3.808E-03	0.05%

Table 19, neutron detection probability for a 4 wt.%, 45 GWd/tU, 20-years cooled BWR assembly measured in the PNAR instrument for 6 different situations. The assembly was in 3 different physical locations. In each of those locations the detection probability was simulated with or without a Cd-liner present.

In Table 20, nine different PNAR Ratio values are listed for the 3 wt.%, 30 GWd/tU, 20-yr cooled assembly. The PNAR Ratios were calculated for all possible assembly locational permutations given the data in Table 18. For example, given the case of the assembly centered in the instrument for the Cd-liner present, the PNAR Ratio was then calculated for three different "without Cd-liner" cases: assembly centered, assembly against the side of the detector wall or in the corner. The data in six of the rows are highlighted yellow to indicate the rows used to calculate the PNAR Ratio for the cases when the assembly did not move between the simulation of the numerator and the denominator of the PNAR Ratio. Table 21 is identical to Table 20 except that the simulations were performed with the isotopic mixture representative of a 4 wt.%, 45 GWd/tU, 20-yr cooled BWR assembly.

X-offset (mm)	Y-offset (mm)	PNAR Ratio	PNAR Ratio Uncertainty 1-sigma
0, 0	0, 0	1.1522	0.0008, 0.07%
0, 5	0, 0	1.1513	0.0008, 0.07%
0, 5	0, 5	1.1511	0.0008, 0.07%
5, 0	0, 0	1.1534	0.0008, 0.07%
5, 5	0, 0	1.1526	0.0008, 0.07%
5, 5	0, 5	1.1524	0.0008, 0.07%
5, 0	5, 0	1.1540	0.0008, 0.07%
5, 5	5, 0	1.1531	0.0008, 0.07%
5, 5	5, 5	1.1529	0.0008, 0.07%

Table 20, PNAR Ratio for a 3 wt.%, 30 GWd/tU, 20-years cooled BWR assembly measured in the PNAR instrument. The PNAR Ratio was calculated for all possible assembly locational permutations as described in the text. For the X-offset and Y-offset values, the coordinate of the "with Cd-liner" case is listed first and the "without Cd-liner" case is listed second.

X-offset (mm)	Y-offset (mm)	PNAR RATIO	PNAR Ratio Uncertainty 1-sigma
0, 0	0, 0	1.1475	0.0008, 0.07%
0, 5	0, 0	1.1473	0.0008, 0.07%
0, 5	0, 5	1.1472	0.0008, 0.07%
5, 0	0, 0	1.1480	0.0008, 0.07%
5, 5	0, 0	1.1478	0.0008, 0.07%
5, 5	0, 5	1.1477	0.0008, 0.07%
5, 0	5, 0	1.1494	0.0008, 0.07%
5, 5	5, 0	1.1492	0.0008, 0.07%
5, 5	5, 5	1.1492	0.0008, 0.07%

Table 21,PNAR Ratio for a 4 wt.%, 45 GWd/tU, 20-years cooled BWR assembly measured in the PNAR instrument. The PNAR Ratio was calculated for all possible assembly locational permutations as described in the text. For the X-offset and Y-offset values, the coordinate of the "with Cd-liner" case is listed first and the "without Cd-liner" case is listed second.

The following 4 tables, Table 22 to Table 25, are identical to the previous 4 tables, except that these later tables are for VVER fuel. Given that it is VVER fuel and there are six sides, the three assembly positions simulated are slightly different than were simulated for the BWR fuel. In Table 22 the first two lines are for a centered assembly; the next two lines are for the assembly slid directly up in Figure 4 such that the assembly would be against the upper most side of the detector and centered on that side. The final two lines of the table are for when the assembly is pushed to the left until it is wedged into a 60-degree corner of the detector.

X-offset (mm)	Y-offset (mm)	Cd Liner	Detection Probability	MCNP5 Uncer. 1-sigma
0	0	YES	1.854 E-03	0.07%
0	0	NO	2.058 E-03	0.07%
0	3	YES	1.851 E-03	0.07%
0	3	NO	2.059 E-03	0.07%
3.4	0	YES	1.851 E-03	0.07%
3.4	0	NO	2.062 E-03	0.07%

Table 22, neutron detection probability for a 3 wt.%, 30 GWd/tU, 20-years cooled VVER assembly measured in the PNAR instrument for 6 different situations. The assembly was in 3 different physical locations. In each of those locations the detection probability was simulated with or without a Cd-liner present.

X-OFFSET (MM)	Y-OFFSET (MM)	Cd LINER	DETECTION PROBABILITY	MCNP5 UNCER. 1-SIGMA
0	0	YES	1.846 E-03	0.07%
0	0	NO	2.051 E-03	0.07%
0	3	YES	1.847 E-03	0.07%
0	3	NO	2.055 E-03	0.07%
3.4	0	YES	1.845 E-03	0.07%
3.4	0	NO	2.057 E-03	0.07%

Table 23, neutron detection probability for a 4 wt.%, 45 GWd/tU, 20-years cooled VVER assembly measured in the PNAR instrument for 6 different situations. The assembly was in 3 different physical locations. In each of those locations the detection probability was simulated with or without a Cd-liner present.

X-OFFSET (MM)	Y-OFFSET (MM)	PNAR RATIO	PNAR RATIO UNCERTAINTY 1-SIGMA
0, 0	0, 0	1.1123	0.0011, 0.10%
0, 0	0, 3	1.1128	0.0011, 0.10%
0, 3.4	0, 0	1.1148	0.0011, 0.10%
0, 0	3, 0	1.1119	0.0011, 0.10%
0, 0	3, 3	1.1124	0.0011, 0.10%
0, 3.4	3, 0	1.1144	0.0011, 0.10%
3.4, 0	0, 0	1.1114	0.0011, 0.10%
3.4, 0	0, 3	1.1119	0.0011, 0.10%
3.4, 3.4	0, 0	1.1139	0.0011, 0.10%

Table 24, PNAR Ratio for a 3 wt.%, 30 GWd/tU, 20-years cooled VVER assembly measured in the PNAR instrument. The PNAR Ratio was calculated for all possible assembly locational permutations as described in the text. For the X-offset and Y-offset values, the coordinate of the "with Cd-liner" case is listed first and the "without Cd-liner" case is listed second.

X-OFFSET (MM)	Y-OFFSET (MM)	PNAR RATIO	PNAR RATIO UNCERTAINTY 1-SIGMA
0, 0	0, 0	1.1109	0.0011, 0.10%
0, 0	0, 3	1.1132	0.0011, 0.10%
0, 3.4	0, 0	1.1142	0.0011, 0.10%
0, 0	3, 0	1.1107	0.0011, 0.10%
0, 0	3, 3	1.1131	0.0011, 0.10%
0, 3.4	3, 0	1.1141	0.0011, 0.10%
3, 0	0, 0	1.1115	0.0011, 0.10%
3.4, 0	0, 3	1.1138	0.0011, 0.10%
3.4, 3.4	0, 0	1.1148	0.0011, 0.10%

Table 25, PNAR Ratio for a 4 wt.%, 45 GWd/tU, 20-years cooled VVER assembly measured in the PNAR instrument. The PNAR Ratio was calculated for all possible assembly locational permutations as described in the text. For the X-offset and Y-offset values, the coordinate of the "with Cd-liner" case is listed first and the "without Cd-liner" case is listed second.

Appendix D: Counting Statistics Analysis

This appendix gives details on the topic of the neutron count rate in the context of the PNAR design. As was stated at the beginning of this report, the instrument that is the subject of the current simulation research is not expected to be the final design. Rather the instrument simulated is expected to be close to a final design; it is expected that final recommendations can be made that build upon the current design.

The following topics are analyzed in this appendix: (1) the relative change in the count rate anticipated for the fuel in Finland given the variation in burnup and cooling time. (2) The maximum, typical and low count rate statistics for a PNAR instrument given the relative neutron intensity if the PNAR system is designed to have the maximum count rate recommended for the detection system when the most intense assembly is measured.

In Table 26 the absolute neutron emission rate is listed for three 17x17 PWR assemblies which were irradiated to burnup levels of 15, 30, 45 GWd/tU for cooling times of 20, 40, 60 and 100 years. Each assembly started with an initial enrichment of 4 wt.% ^{235}U. These results were obtained using the formulas associated with Figures 46, 47 and 48 in the publication by Weldon et al. [20] This publication was selected because (1) a general formula for the total neutron emission as a function of cooling time was provided and (2) neutrons from both spontaneous fission and (α,n) emission were included. The inclusion of the (α,n) term is considered important because this term becomes a significant term to the total neutron emission when the burnup is particularly low or the cooling time is particularly long. As our goal is to quantify the neutron emission at the extremes of what will be measured, we are interested in this low burnup, long cooling time case. The 100-year cooling time was added as an extreme limit. Two non-ideal features of the assemblies used by Weldon et al. in the context of the current work are that (1) they all have the same initial enrichment of 4 wt.% ^{235}U. Ideally the low burnup assemblies would have a low initial enrichment commensurate with their burnup. (2) The assemblies are all PWR. A duplicate analysis using BWR would be preferable. Yet, in the publication by Hu at al. [24], the neutron emission source term is compared between PWRs and BWRs. The two fuel types are close enough in terms of the intensity of the total neutron source term that using PWR data for estimating the overall variation in BWR fuel neutron source term is considered acceptable for providing a rough overall count rate estimate. Of note in the BWR context is that the neutron energy spectrum varies along the axial length of the assembly as the void ratio varies. If an accurate neutron emission from a section of a BWR assembly is of interest, detailed irradiation calculations are needed. In this current work, we are interested in a rough estimate of the mid-plane emission, a factor of 2 inaccuracy is acceptable.

BURNUP (GWD/TU)	NEUTRON EMISSION FOR 20 YEAR COOLING TIME (N/S)	NEUTRON EMISSION FOR 40 YEAR COOLING TIME (N/S)	NEUTRON EMISSION FOR 60 YEAR COOLING TIME (N/S)	NEUTRON EMISSION FOR 100 YEAR COOLING TIME (N/S)
15	1.40E+06	9.74E+05	6.79E+05	3.31E+05
30	2.53E+07	1.28E+07	6.50E+06	1.67E+06
45	1.46E+08	7.11E+07	3.46E+07	8.20E+06

Table 26, list of total neutron emission for 12 assemblies as a function of burnup and cooling time for a 4 wt.%, 17x17 PWR assembly obtained from Weldon et al.

Table 27 lists the normalized variation in the total neutron emission as a function of cooling time and burnup. For the 3 burnup values listed in Table 26, the 40, 60 and 100-year cooling times are normalized to the 20-year cooling time of that same burnup; the three cases listed in Table 26 are highlighted yellow in Table 27. We note from the three rows of data for these three burnup values that the rate of decrease in the neutron emission rate as a function of cooling time is greatest for the 45 GWd/tU case and subsequently less for the lower burnup cases, particularly the 15 GWd/tU case. This is due to the significant contribution of (α,n) produced neutrons in this low burnup case. The 45 GWd/tU case decreases in intensity with essentially the decay rate of ^{244}Cm as the neutron intensity of the 20-year cooled case is 97.3% from ^{244}Cm as indicated in Figure 58 of Weldon et al.

The normalized neutron intensity of the 17, 25, 35, 55 GWd/tU burnup values in Table 27 were calculated from the 15, 30 and 45 GWd/tU normalized data. The simplistic assumption was made in calculating the values for the 17, 25, 35 GWd/tU cases that the contribution from (α,n) and spontaneous fission varied linearly with burnup between the 15, 30 and 45 GWd/tU cases; the 55 GWd/tU case was assumed to be identical to the 45 GWd/tU case as the neutron emission for both these cases is overwhelmingly dominated by ^{244}Cm. This simplifying assumption was made to provide a rough estimate of the total neutron emission in the absence of more accurate simulations.

BURNUP (GWD/TU)	NORMALIZED NEUTRON EMISSION FOR 20 YEAR COOLING TIME	NORMALIZED NEUTRON EMISSION FOR 40 YEAR COOLING TIME	NORMALIZED NEUTRON EMISSION FOR 60 YEAR COOLING TIME	NORMALIZED NEUTRON EMISSION FOR 100 YEAR COOLING TIME
15	1	0.698	0.487	0.237
17	1	0.674	0.458	0.216
25	1	0.570	0.333	0.123
30	1	0.507	0.257	0.066
35	1	0.500	0.250	0.063
45	1	0.487	0.237	0.056
55	1	0.487	0.237	0.056

Table 27, normalized variation in the neutron emission intensity for each burnup value as a function of cooling time.

In Table 28, five burnup values that span the burnup range of interest for BWR assemblies in Finland are listed. The highest and lowest values are explicit to the Finnish case, while the intermediate values were selected to give some resolution to the expected assemblies in between the extreme values. The middle column in this table is the product of the burnup value of that row raised to the fourth power multiplied by the normalization value in Table 27 (NORM_T22) appropriate for the burnup and cooling time; In the case of Table 28 all the NORM_T22 values are 1.0 because all the data in Table 28 have a cooling time of 20 years. The values in the final column of Table 28 were calculated by normalizing the values in the middle column to the lowest burnup case.

We see from the data in Table 28 is that the neutron emission rate is expected to vary by a factor of ~110 due to the variation in burnup only. In Table 29, Table 30 and Table 31 we see the same calculations for cooling times of 40, 60 and 100-years provide variation of 79, 53 and 29 over the entire 17 to 55 GWd/tU burnup range for each of those cooling times respectively. The reduction in the range of variation as a function of cooling time is due to the increased contribution of (α,n) and ^{240}Pu terms with cooling time.

Burnup (GWd/tU)	Burnup^4 * Norm_T22	Normalizated BU^4*Norm_T22
17	83,521	1.0
25	390,625	4.7
35	1,500,625	18.0
45	4,100,625	49.1
55	9,150,625	110

Table 28, estimation of the variation in neutron emission intensity as a function of burnup assuming the neutron emission varies as the burnup to the fourth power and using the cooling time corrections listed in Table 7. All fuel is 20-years cooled.

Burnup (GWd/tU)	Burnup^4 * Norm_T22	Normalization BU^4* Norm_T22
17	56,276	1.0
25	222,775	4.0
35	750,306	13.3
45	1,995,988	35.5
55	4,454,087	79.1

Table 29, estimation of the variation in neutron emission intensity as a function of burnup assuming the neutron emission varies as the burnup to the fourth power and using the cooling time corrections listed in Table 7. All fuel is 40-years cooled.

Burnup (GWd/tU)	Burnup^4 * Norm_T22	Normalization BU^4* Norm_T22
17	40,654	1.0
25	130,218	3.2
35	375,281	9.2
45	971,552	23.9
55	2,168,037	53.3

Table 30, estimation of the variation in neutron emission intensity as a function of burnup assuming the neutron emission varies as the burnup to the fourth power and using the cooling time corrections listed in Table 7. All fuel is 60-years cooled.

Burnup (GWd/tU)	Burnup^4 * Norm_T22	Normalization BU^4* Norm_T22
17	19,788	1.0
25	84,198	4.3
35	184,415	9.3
45	270,128	13.7
55	573,086	29.0

Table 31, estimation of the variation in neutron emission intensity as a function of burnup assuming the neutron emission varies as the burnup to the fourth power and using the cooling time corrections listed in Table 9. All fuel is 100-years cooled.

The end goal of the calculations illustrated in Table 26 to Table 31 is to calculate the variation in the count rate between the weakest neutron emitting assembly, a 17 GWd/tU cooled for 60 years, and the strongest neutron emitting assembly, a 55 GWd/tU cooled for 20 years. From Table 26 to Table 28 we see that this is the ratio of 40,654 : 9,150,625 **which is 1 : 225**. Hence, we expect the strongest assembly to emit ~225 more neutrons than the weakest. A more typical assembly ~35 GWd/tU cooled for 40 years will emit (40,654 : 750,306) ~19 times more neutrons than the weakest assembly and (750,306: 9,150,625) ~12 times less than the strongest assembly.

The calculations performed in this section fit into the larger context of informing the analysis of the count time and detector efficiency. The first step in this process involved quantifying the neutron count rate difference between the most and least intense assemblies. The second step is to assume that the neutron efficiency can be designed such that the assembly with the largest neutron emission rate can produce the highest count rate possible for the utilized neutron detection technology. Such a system would be able to measure all the assemblies that may need to be measured and have the optimal counting statistics.

In Table 32, seven count rates are listed along with the statistics resulting from an assumed 2-minute counting interval. Two minutes was assumed to be the counting interval because approximately 5 minutes are anticipated for the Passive Gamma Emission Tomography detector, which is anticipated to be part of the integrated NDA instrument. Hence, two minutes for two PNAR measurements leaves one minute to move the Cd-liner so that both measurement systems can finish measuring at approximately the same time.

The highest measurable count rate was taken to be 2e5 counts/s. This value was calculated based upon two assumptions/factors: (1) four detectors will be used for a given PNAR section, (2) the recommendation of Nathan Johnson of GE Reuter-Stokes was that a 5e4 counts/s per tube is a reasonable upper count rate limit; a count rate that will results in approximately a 5% dead time. This is a "comfortable" upper limit in that a doubling of the count rate above this limit is manageable with a dead-time correction.

Count Rate without Cd (cts/s)	Total Counts in 120 seconds (cts)	Uncertainty in Total Counts 120 seconds (cts)	Percentage Uncertainty in Total Counts 120 seconds
11	1,361	37	2.71%
113	13,612	117	0.86%
889	106,626	327	0.31%
1,134	136,116	369	0.27%
11,343	1,361,160	1,167	0.086%
113,430	13,611,600	3,689	0.027%
200,000	24,000,000	4,899	0.020%

Table 32, for a wide range of potential count rates obtained with the PNAR detector when no Cd layer is present, the counting statistics uncertainty is listed. The yellow highlighted numbers are the high and low count rates for an optimally designed PNAR instrument; the green highlight is for a typical assembly.

The count rates in Table 33 were calculated by dividing the count rates in Table 32 by a factor of 1.1343 because this is the PNAR Ratio for a 45 GWd/tU, 4 wt%., 20-year cooled assembly as listed in Table 2. The 45 GWd/tU, 4 wt%., 20-year cooled assembly was selected because it represents a nearly fully irradiated assembly for which the difference between the with and without Cd cases will be small; hence, producing a situation that is both typical and less favorable from a statistical perspective.

Count Rate with Cd (cts/s)	Total Counts in 120 seconds (cts)	Uncertainty in Total Counts 120 seconds (cts)	Percentage Uncertainty in Total Counts 120 seconds
10	1,200	35	2.89%
100	12,000	110	0.91%
783	94,002	307	0.33%
1,000	120,000	346	0.29%
10,000	1,200,000	1,095	0.091%
100,000	12,000,000	3,464	0.029%
176,320	21,158,424	4,600	0.022%

Table 33, for a wide range of potential count rates obtained with the PNAR detector when a Cd layer is present, the counting statistics uncertainty is listed. The yellow highlighted numbers are the high and low count rates for an optimally designed PNAR instrument while the green highlight is for a typical assembly.

In Table 34 the count rates listed in Table 32 and Table 33 were combined to calculate the PNAR Ratio and the uncertainty in that ratio. Two rows are highlighted yellow in Table 34. The bottom yellow highlighted row represents the highest count rate case as was described earlier. The other yellow highlighted row has a count rate that is 225 lower than the highest count rate case; hence this row represents the statistics expected for the weakest assembly to be measured provided the detector was designed to optimally measure the strongest assembly to be measured. The row highlighted in green represents the statistics to be expected for a typical assembly.

Count Rate without Cd (cts/s)	PNAR Ratio with absolute uncertainty	Percentage uncertainty in PNAR Ratio
11	1.1343 +/- 0.0449	3.96%
113	1.1343 +/- 0.0142	1.25%
889	1.1343 +/- 0.0051	0.45%
1,134	1.1343 +/- 0.0045	0.40%
11,343	1.1343 +/- 0.0014	0.13%
113,430	1.1343 +/- 0.0004	0.04%
200,000	1.1343 +/- 0.0003	0.03%

Table 34, the PNAR results calculated using the results listed in Table 11 and Table 12. The yellow highlighted numbers are the high and low count rates for an optimally designed PNAR instrument while the green highlight is for a typical assembly.

Appendix E: MCNP6™ Input Files Provided

The following is a list of the MCNP6™ files provided to STUK and HIP. For each title listed an input file, output file and mctal file are provided. An EXCEL file was provided with the name "BWR and VVER – PNAR results – 2017" that contained a more detailed description of each file as well as the tally results.

1. BWR Neutron Files
   - *a)* 42 base-simulations that varied in initial enrichment, burnup and cooling time were simulated with names that progressed from PNAR-F33b, PNAR-F34b … PNAR-F68b. Six of these files were simulated a second time with the inclusion of the "nonu" card; the file names have "–nonu" added to the end.
   - *b)* 3 simulations were performed for which the Cd-liner length was doubled from 0.74 m to 1.48 m. Their file names have "-longCd" added to the names used with the base-simulation.
   - *c)* 6 simulations were performed for which the density of the water between the assembly box and detector walls was doubles to approximate a larger water gap. The files names have "-doubleH2O" added to the end of the names used with the base-simulation.
   - *d)* 3 simulations for which the thickness of the Cd-liner was varied. The text "-quarterCd," "-halfCd" and "-doubleCd" were added to the end of the PNAR-F43b" name.
   - *e)* 4 simulations were performed to estimate the response of fission chambers. These files have the suffix "fc_" added to the beginning of the names used with the base-simulation.
   - *f)* 4 simulations were performed to estimate the response of boron tubes. These files have the suffix "bt_" added to the beginning of the names used with the base-simulation.
   - *g)* **Summary: A total of 62 BWR simulations** were performed by Dr. Tobin using MCNP6™. Additional simulations were performed by Dr. Peura using MCNP5, some of which are presented in this report; these files were provided separately by Dr. Peura.
2. VVER Neutron Files
   - *a)* 42 base-simulations that varied in initial enrichment, burnup and cooling time were simulated with names that progressed from PNAR-F33v, PNAR-F34v … PNAR-F68v. Six of these files were simulated a second time with the inclusion of the "nonu" card; the file names have "–nonu" added to the end.
   - *b)* 21 supplementary base-simulations were performed to test out a second "low multiplying" setup. For this second set of low multiplying simulations, borated water was replaced with PE.
   - *c)* 3 simulations were performed for which the Cd-liner length was doubled from 0.74 m to 1.48 m. Their file names have "-longCd" added to the names used with the base-simulation.
   - *d)* 6 simulations were performed for which the density of the water between the assembly box and detector walls was doubles to approximate a larger water gap. The files names have "-doubleH2O" added to the end of the names used with the base-simulation.
   - *e)* 3 simulations were performed to test the impact of using borated PE instead of regular PE in the design of the low multiplying setup. Their file names have "-borated-poly" added to the names used with the base-simulation.
   - *f)* 12 simulations were performed to estimate the impact of the boron in the water varying from 14 g of boric acid to 13 g or 15 g. Their file names have "-13g" or "-15g" added to the names used with the base-simulation.

g) 20 simulations were performed to estimate the performance of the PNAR technique in air.

h) **Summary: A total of 107 VVER neutron simulations** were performed by Dr. Tobin using MCNP6™. Additional simulations were performed by Dr. Peura using MCNP5, some of which are presented in this report; these files were provided separately by Dr. Peura.

3. Gamma files:

a) For the BWR gamma simulations, an iterative process was followed by which the ^{3}He tube was moved within the lead block or the amount of lead was changed until the desired dose to the tube was obtained. For this reason, only the result was saved. This final file has the name PNAR-F25.

b) For the VVER gamma simulations a similar process was followed, but three of the earlier results were saved. The result is in the file VVER-PassiveG-04, while the earlier results were VVER-PassiveG-01, VVER-PassiveG-02, VVER-PassiveG-03.

4. A total of 175 input, output and mctal files were provided.